iScience

Article

Geoarchaeological insights into a Neolithic combustion feature from Abric del Xicotó (northeastern Iberia)

Graphical abstract

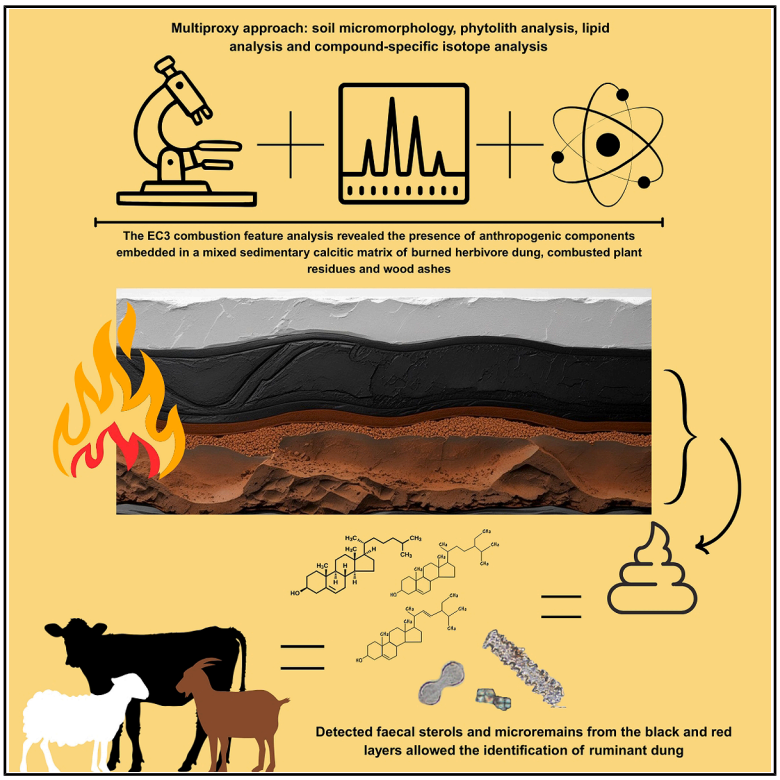

Highlights

- Evidence for ruminant dung is detected in the EC3 combustion feature at Abric del Xicotó
- EC3 is a single combustion event, unlike *fumier* deposits in Iberian Neolithic sites
- Ruminants sought shelter at Abric del Xicotó possibly during late spring or early summer

Authors

Enrique Fernández-Palacios, Natalia Égüez, Cynthia González-Olivares, Antonio V. Herrera-Herrera, Carolina Mallol, Xavier Mangado, Marta Sánchez de la Torre

Correspondence

efernand@ull.edu.es (E.F.-P.), natalia.eguez@ipna.csic.es (N.É.)

In brief

Archeology; Biochemical analysis; Biogeoscience

Fernández-Palacios et al., 2025, iScience *28*, 113293
September 19, 2025
https://doi.org/10.1016/j.isci.2025.113293

CellPress

iScience

CellPress
OPEN ACCESS

Article

Geoarchaeological insights into a Neolithic combustion feature from Abric del Xicotó (northeastern Iberia)

Enrique Fernández-Palacios,[1,2,8,*] Natalia Égüez,[1,3,4,5,8,9,*] Cynthia González-Olivares,[4,5] Antonio V. Herrera-Herrera,[1,6] Carolina Mallol,[1,2,7] Xavier Mangado,[4,5] and Marta Sánchez de la Torre[4,5]

[1]Archaeological Micromorphology and Biomarkers Laboratory (AMBI Lab), Instituto Universitario de Bio-Orgánica Antonio González, Universidad de La Laguna, 38206 Tenerife, Spain
[2]Departamento de Geografía e Historia, Facultad de Humanidades, Universidad de La Laguna, 38200 Tenerife, Spain
[3]Departamento de Ciencias de la Vida y de la Tierra, Instituto de Productos Naturales y Agrobiología, Consejo Superior de Investigaciones Científicas (IPNA-CSIC), 38206 Tenerife, Spain
[4]SERP (Seminari d'Estudis i Recerques Prehistòriques). Universitat de Barcelona, 08001 Barcelona, Spain
[5]IAUB (Institut d'Arqueologia de la Universitat de Barcelona). Universitat de Barcelona, 08001 Barcelona, Spain
[6]Departamento de Química, Facultad de Ciencias, Universidad de La Laguna, 38206 Tenerife, Spain
[7]Interdisciplinary Center for Archaeology and the Evolution of Human Behaviour (ICArEHB), Universidade do Algarve, Campus de Gambelas, 8005-139 Faro, Portugal
[8]These authors contributed equally
[9]Lead contact
*Correspondence: efernand@ull.edu.es (E.F.-P.), natalia.eguez@ipna.csic.es (N.É.)
https://doi.org/10.1016/j.isci.2025.113293

SUMMARY

The Neolithic was a period of important cultural transformations across different regions. Applying state-of-the-art geoarchaeological techniques to archaeological sites from this period has shown to contribute relevant data on site formation processes and occupation dynamics. Combined microcontextual and biomolecular analysis of archaeological combustion features helps us approach fuel use, often associated to dung residues in Neolithic contexts, which offer an insight into herding strategies. Here, we present micromorphological, microremains (fecal spherulites, ash pseudomorphs, and phytoliths), and biomarker data (*n*-alkanes, fecal sterols, and bile acids) obtained from a Neolithic combustion feature at Abric del Xicotó (Alòs de Balaguer, Lleida, Spain). Preliminary data shed light on the functionality of the combustion feature, the presence of husbandry activity at the rockshelter, and the nature of the animals and their diet. This research adds detail to the existing Neolithic archaeological record of the northeastern Iberian Peninsula.

INTRODUCTION

The first arrival of agricultural and pastoralist societies in the Iberian Peninsula is known to have occurred around 7700 BP, involving human migrations across and through the Pyrenees and along the Mediterranean coastline and/or the Ebro river.[1–3] This period witnessed the migration of farming populations that brought agriculture and animal husbandry to the northeastern regions that were previously uninhabited or sparsely populated.[4] It is suggested that neolithization may not have been as uniform as previously assumed; instead, it appears to have affected distinct biotopes independently (i.e., coastal plains to high mountains) during both earlier phases and more developed stages.[5] In fact, the distribution of Cardial and Epicardial wares (a typological marker of the first stages of neolithization) reflects such spatial patterning. For example, in the case of the Segre-Ebro Valley area, there is initial evidence of Epicardial ceramics, in contrast to the coastal and pre-coastal area of the northeast of Iberia, with initial Cardial evidence.[6,7] The neolithization process in this region involved intensified landscape transformations, such as woodland openings for farming and grazing of domesticates.[8,9] In this regard, common husbandry practices in this region show sheep, goat, cattle, and pig exploitation, with vertical movements of ovicaprine herds.[10,11]

The presence of pastoralist groups in the Iberian Pre-Pyrenees during the Neolithic, Chalcolithic, and Bronze Age has been commonly documented and exemplified through stone enclosures and *fumier* sequences (i.e., alternating layers of burned and unburned herbivore dung mixed with heterogeneously burned vegetal matter) found within rockshelters and caves mostly used for livestock corralling purposes and often used as a transitory settlement during the seasonal movement of herds.[12,13] Well-documented sites in this area showing pastoral occupation are Cova Colomera (Late Cardial Neolithic to Late Roman),[12,14,15] Cova Gran de Santa Linya (Middle Palaeolithic to Early Bronze Age),[13,16] Cueva de Chaves (Upper Palaeolithic to Early Neolithic),[17] Cova Bonica (Early Neolithic),[18] Can Sadurní (Middle Neolithic),[19,20] Els Trocs (Early to Middle

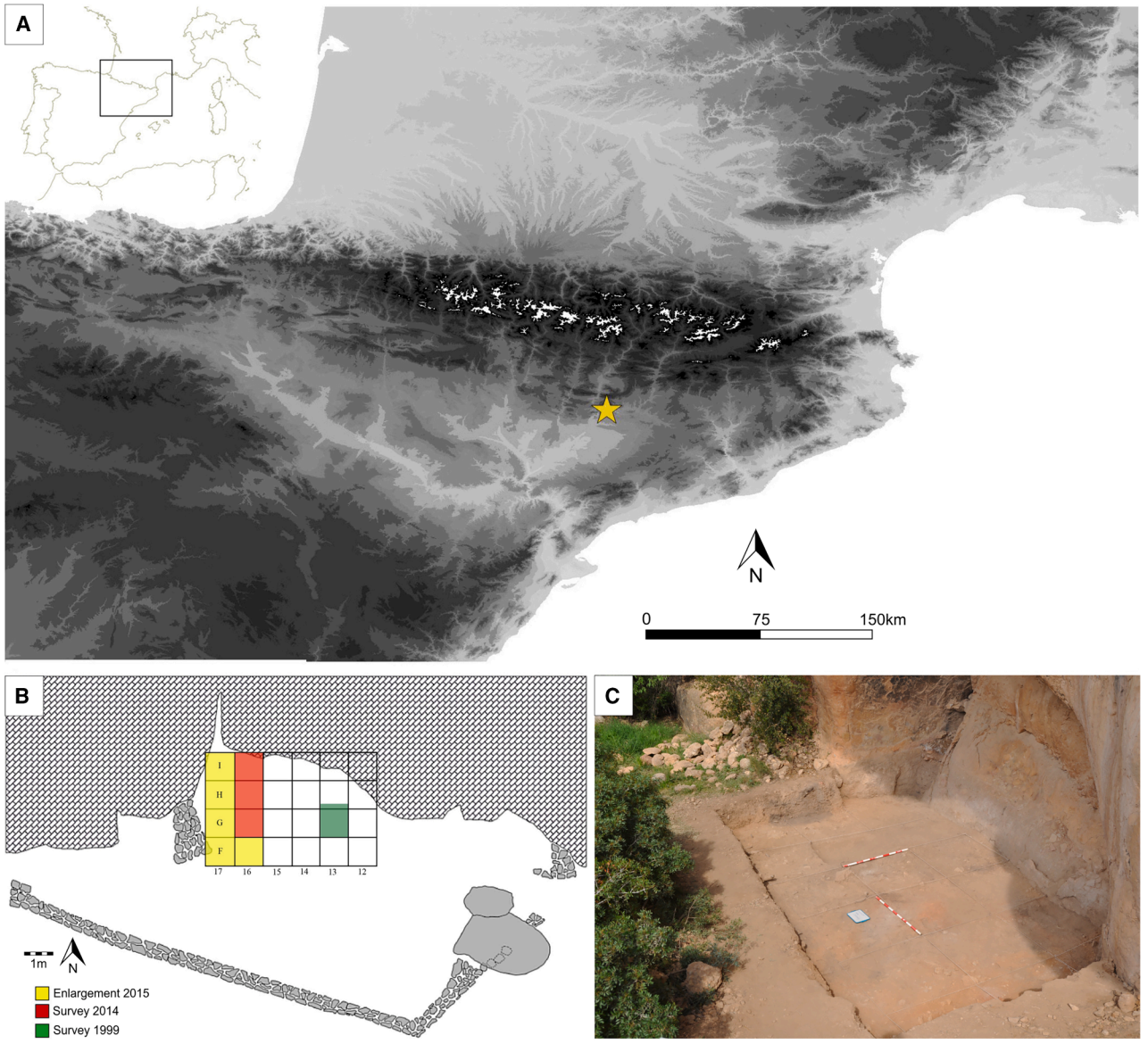

Figure 1. Setting and view of Abric del Xicotó

(A) Location of Abric del Xicotó.

(B) Archaeological surveys and excavations conducted until 2016, when the samples concerning this study were taken.

(C) Photography of the rockshelter and excavated area by the end of 2017 campaign.

Neolithic),[21] Coro Trasito (Early Neolithic to Middle Bronze Age),[22,23] or Cova del Parco (Early Neolithic).[24,25]

In such cave settings, the application of archaeological soil micromorphology has been key to characterizing the site formation processes and, thus, understanding the use of space.[13,14,21,26–29] Herbivorous dung identification through micromorphology usually relies on the presence of preserved microfragments of coprolites or fecal spherulites. There are, however, other microscopic features associated with depositional contexts related to past livestock corralling activities, including microlaminations, trampling, the abundance of silica phytoliths, and post-depositional features such as phosphate nodules, phosphate-rich minerals, dissolution processes, and bioturbation.[30–32] On the other hand, the quantification of microremains, including phytoliths, fecal spherulites, and ash pseudomorphs in bulk sediment has been applied in (ethno) archaeological contexts to determine fuel sources[33–38] and recently also in *fumiers* to support micromorphological observations, differentiate between burned layers dominated by dung and those showing dominance of wood-derived ashes, and address deposited plant matter composition.[39,40]

More recently, biomarker analyses on sediments have also been performed in Iberian Neolithic-Bronze Age and Canarian pre-Hispanic *fumier* sequences, mostly concerning fecal

Table 1. Radiocarbon dates obtained from charcoals recovered at different combustion features (EC) and posthole (E11) from Abric del Xicotó

Lab Code	Level	Origin	Age (y)	± y	$\delta^{13}C$ (‰)	cal BP (2 σ)
Beta-382458	I	EC3	6,210	40	−24.6	7251–6990
Beta-493571	III	EC12	7,900	30	−20.1	8977–8596
CNA-5703	III	EC12	7,989	42	−20.6	9000–8646
CNA-6399	III	EC14	8,069	38	−22.2	9123–8776
CNA-6400	III	EC14	7,911	39	−23.2	8981–8598
CNA-6401	III	E11	7,973	37	−21.3	8994–8649

Calibrated data have been calculated with OxCal v.4.4[51] following the IntCal20 curve.[52]

biomarker analysis[41–45] and *n*-alkane analysis.[28,45] The identification of sterols and bile acids can help us identify animal species being herded[46–48] and thus further approach livestock management practices among prehistoric pastoral groups.

Abric del Xicotó, a rockshelter site featuring a stratified sequence dated to between the Mesolithic and the Bronze Age, holds significant importance toward our understanding of the earliest agro-pastoral communities in the northeastern Iberia region, for which the archaeological record is scanty. The site has yielded combustion structures, post holes, and other sedimentary features in addition to pottery sherds, lithic and bone artifacts, and shell ornaments, from what possibly represents seasonal or sporadic occupations due to the low amount of recovered remains.[6] In this article, we conduct a microcontextual interdisciplinary study of one of the combustion structures from Xicotó rockshelter. Our aim is to identify the source of the burned organic matter through a combination of micromorphology, microremains, and biomolecular analysis. Specifically, we seek to determine if there is herbivore excrement within the burned sediment as evidence of animal presence at the site. The identification of animal husbandry-related activities has ecological, economic, and social implications. Thus, clarifying this issue will contribute to our understanding of early Neolithic societies in the region.

The archaeological site and field sampling

Abric del Xicotó (Alòs de Balaguer, Lleida, Spain) is an archaeological site located at the southern slope of the Sant Mamet mount, which constitutes the first Pre-Pyrenean mountain ranges located near the Catalan Central Depression. The site lies at 368 m asl and at around 100 m above the current Segre riverbed within a calcareous and conglomerate landscape with pH values of sediments between 8 and 9 (measured with a portable pH meter). The rockshelter has a maximum length of 18 m in its E-W direction and 8 m in the N-S axis (Figure 1).

The site was first spotted during geoarchaeological surveys carried out in the river Segre in 1996.[49] The first archaeological works were done in 1999 and consisted of a 4 m^2 stratigraphic test pit in the center of the rockshelter, which uncovered several sedimentary layers containing archaeological remains. Within the archaeological evidence recovered, there were some faunal remains, pottery, and lithic artifacts. In 2013, the archaeological work was restarted and still continues today, with an extended excavation area of 24 m^2. Up to now, three levels have been detected along the sedimentary sequence.

(1) Level I: this level is found below a mixed level, evidencing human frequentation during the Bronze Age. Level I consists of a 40 cm deep sedimentary package displaying hearths and pits. The recovered archaeological assemblage includes impressed pottery and double-bevel geometric lithic tools, which suggest a relative chronology from the Early Neolithic.[6] This relative chronology was confirmed by a radiocarbon date from EC3, dated in 7251–6990 cal BP (Table 1 and Figure S1).[50] Firstly, the Early Neolithic occupations were attributed to level II,[6] but the latest studies involving Geographic Information System (GIS) approaches have forced us to include these materials with the Bronze Age occupations as appearing to level I, due to the inexistence of sedimentary changes and mixed Bronze Age and Neolithic archaeological materials.[50]

(2) Level II: this level shows a mixed archaeological assemblage of about 20 cm, including materials recognized in levels I and III, so it has been defined as a transitional level.

(3) Level III: this level is still under excavation, but it seems to correspond to a Middle Mesolithic occupation of the site, indicated by the great amount of notched and denticulated chert artifacts representing the Mesolithic facies known as Notch and Denticulates. The typology of the lithic set is supported by five radiocarbon dates from three different pits, stating a human occupation c. 9100–8600 cal BP (see Table 1 and Figure S1).

Combustion structure EC3 (Figure 2) was first documented in 2014 during the excavation of level I squares H16 and I16 in the western sector close to the rockshelter wall. Later, in 2016, the excavation of the structure continued in H17. Radiocarbon dating performed on charcoal fragments from this combustion structure (7251–6990 cal BP [2 σ]) coincides well in time with the archaeological materials recovered from this level.[6]

An intact and oriented block sample was collected from EC3 in square I17 for micromorphological analysis (Figure 2). Three bulk sediment samples were collected from the leftover profile of EC3 after the removal of the micromorphological block sample. One sample was taken for each of the different visible layers (red, black, and white layers) of the combustion feature for the analysis of calcitic (fecal spherulites and ash pseudomorphs) and siliceous (phytoliths) microremains.

Bulk loose sediment samples were also collected for biomarker and isotopic analysis by subsampling the extracted undisturbed block using sterilized equipment for the red, black, and white layers. Samples for biomarker analysis were kept at −20°C to mitigate bacterial degradation. Finally, a sediment control sample was collected off-site, at a slope 100 m (approx.) south of the site. The aim was to obtain a biosignature of the natural superficial (modern) soil in order to compare it with the archaeological (anthropogenic) sediment.

RESULTS

Field observations

The excavation of EC3 showed a potential pit hearth of oval morphology and concave base of about 110 cm large in the

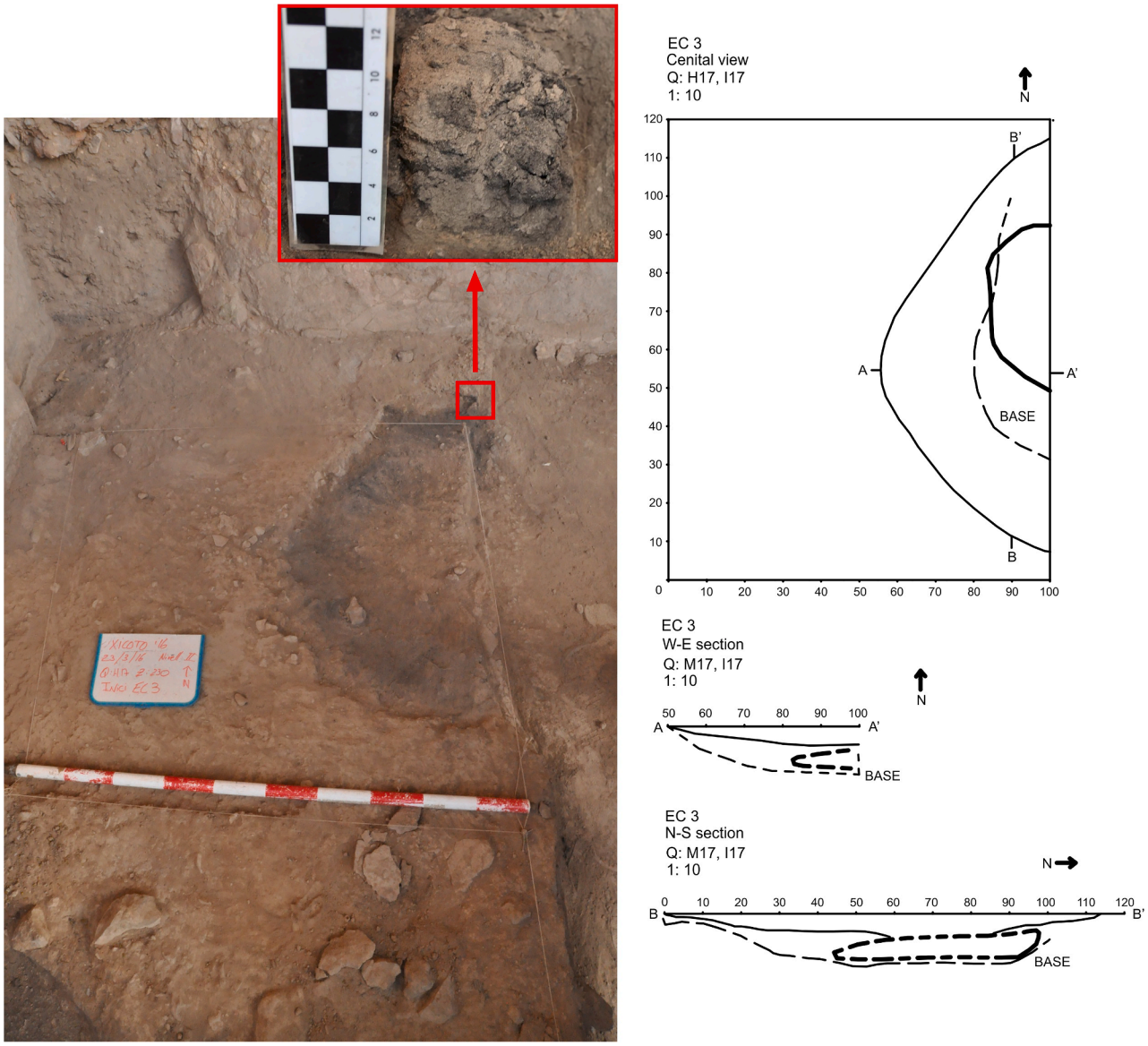

Figure 2. Photograph and planimetry of EC3

The location and photograph of the extracted micromorphological block sample in EC3 is marked in red.

N-S axis and 50 cm in the E-W axis and about 6–7 cm deep (see Figure 2). The absence of external boundary elements such as stones delimiting the external border suggests open-type combustion dynamics. However, in the base, some stone pebbles of less than 5 cm in length were documented, indicating a possible preparation for the base of the hearth. Firstly, attributed to level II and then re-oriented to level I after a GIS approach, the archaeological remains found within the ashy sediment inside the pit were scarce, dealing only with scarce and non-diagnostic lithic and bone remains.

Soil micromorphology

Thin sections EC3-1 and EC3-2 are shown in Figure 3. The lithological composition is mostly based on sand-to-gravel-sized fossiliferous/bioclastic limestone and sandstone fragments, as well as abundant sand-sized quartz. We sometimes observe calcarenite fragments, i.e., stone fragments composed of calcite grains smaller than 2 μm. Furthermore, we observe an allochthonous component of scarce metamorphic rock fragments. Gravel-sized detritic material is often coated by micritic calcite. The groundmass is composed of micritic calcite, showing little or no dissolution features. Anthropogenic and biogenic components such as charcoal, bone, and shell are abundant across the combustion feature (Figure 4).

The microstratigraphic sequence of EC3 is distinctly divided into red, black, and white layers, with a diffuse transition between them, following the typical sequence of a hearth.[53] We have divided this sequence into three microunits corresponding to

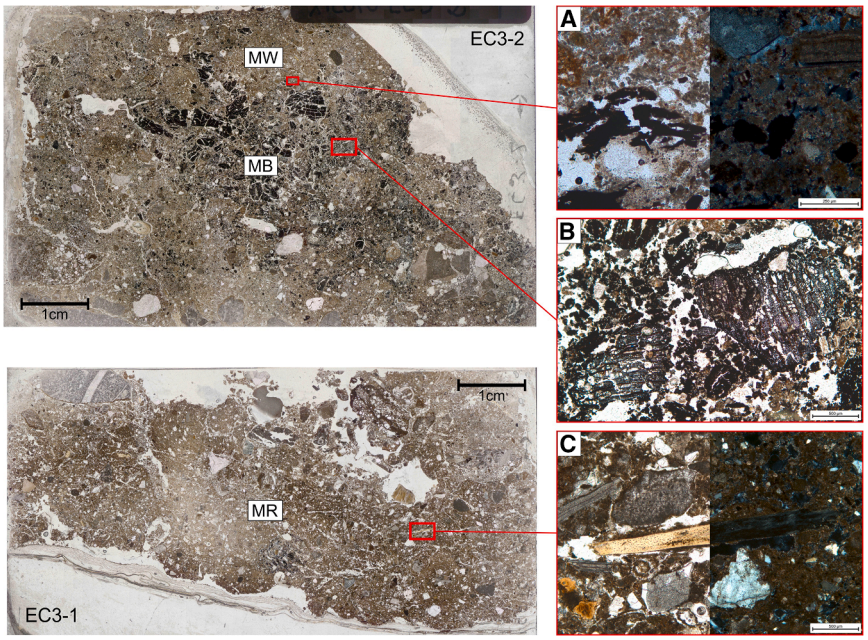

Figure 3. Micromorphological view of documented microunits

Scanned thin sections EC3-1 and EC3-2 (PPL) on the left (scale bars, 1 cm). Microunits red (MR), black (MB), and white (MW) are indicated.

(A) Detail of transitioning area between MB and MW showing abundant rhombic ash pseudomorphs and charred organic material. The left half is in PPL, while the right half in XPL (scale bar, 250 μm).

(B) Broad-leaf tree charcoal fragments (note internal vessels) within a rich charred matter matrix (PPL) (scale bar, 500 μm).

(C) Detail of various anthropogenic and geogenic components found in MR embedded in a micritic calcite matrix. The left half is in PPL and the right half in XPL (scale bar, 500 μm).

PPL, plane-polarized light; XPL, cross-polarized light.

the mentioned layers (see Figure 3). Table S1 summarizes the micromorphological characteristics of each microunit.

Microunit red (MR) is represented in EC3-1 and the lower part of EC3-2. This unit is characterized by a red-brownish-colored groundmass in plane-polarized light (PPL). In cross-polarized light, the *b*-fabric is crystallitic. It displays an angular and platy microstructure, which is locally crumb and/or granular due to bioturbation. It shows a higher detritic unsorted component and less organic and charred material compared to the upper black layer. Some fragments of carbonized plant material are present in the bioturbated areas, possibly translocated from the black layer. Other anthropogenic components, such as bones and shells, are also present in MR (see Figure 3C). Bones possess a yellow-orange color in PPL due to heating (see Figure 4A).[54] A rodent tooth is also visible (Figure 4C). Shell fragments are possibly linked to terrestrial snails (*Cepaea nemoralis*), fluvial (Unionidae), or marine snails (*Columbella rustica* and *Cerithium vulgatum*) as reported in the malacofaunal analysis (see Figure 4D).[55,56] There are clear indications of burning in MR based on the scattered presence of calcitic ash pseudomorphs, charring of various features, and plant remains that show partial carbonization and ash transformation.

Microunit black (MB) is represented across the middle and part of the upper area of EC3-2. We observe a brown-black groundmass and angular blocky to crumb-granular microstructures. The *b*-fabric is mainly undifferentiated, and the matrix is dominated by charcoal fragments and charred organic particles. Transversal charcoal sections indicate broad-leaf trees according to their large vessels (see Figure 3B). We also observe bones and shells embedded in the charred material-rich matrix. Calcitic rhombs, most likely derived from wood ashes, have also been identified, although less concentrated than in the upper white layer. Numerous silt-sized dark-colored spheres and ellipsoids (Figure 4G) are also detected, most likely representing mesofaunal excrements.[57] Their dark color in PPL might indicate that soil mesofauna was consuming and excreting already charred organic matter in the form of pellets.

Microunit white (MW) corresponds to the upper right area of EC3-2. The matrix shows a similar color in PPL to that in MR, although with abundant charred particles. Here, the microstructure is mostly angular blocky but still preserves some crumb-granular areas. There is a high concentration of wood ash rhombic micritic grains as well as calcified plant pseudomorphs (see Figures 3A, 4E, and 4H). The higher birefringence of this layer, in comparison with MB, highlights the calcitic nature of the ashes. Bones in MW appear to have a more intense yellowish-orange color (PPL) than those in MB and MR, possibly related to exposure to higher heating temperatures.[54]

Micromorphological evidence for herbivore dung can be found across all three microunits. We identified aggregates of herbivore dung varying in size from 0.6 mm to 50 μm, displaying a convolute microstructure with internal pores but almost no visible outer rims as is usually documented in coprolite fragments (Figures 5A and 5B). The interior of some of these dung aggregates is rich in phytoliths and fecal spherulites, thus likely being originated by ruminants. However, we also observe fragments of coprolites in which fecal spherulites are absent. Single fecal spherulites are also scattered across the calcitic matrix in all microunits, in both unaltered and darkened states.[58] These are commonly found in association with phytoliths. The decay of dung might also be causing post-depositional formation of phosphatic nodules (Figures 5C, 5D, and 5E).[32]

Calcitic and siliceous microremains

Phytoliths, fecal spherulites, and ash pseudomorphs were present in all microunits (Figure 6), although with varying concentrations. The control sediment also contained phytoliths and fecal spherulites but no ash pseudomorphs. Table 2 shows the estimated amounts of these microremains in EC3 and the control sample. Pseudomorph/spherulite ratio (PSR) values are

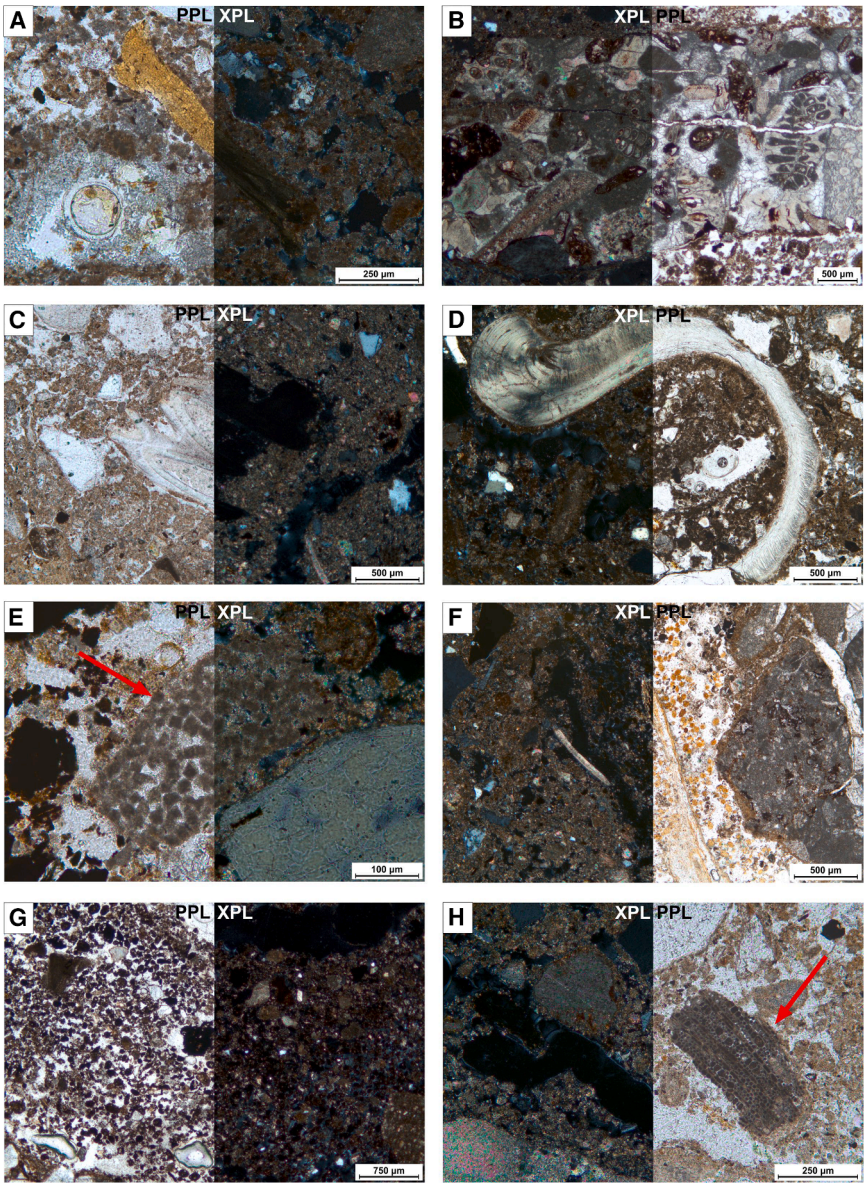

Figure 4. Selection of photomicrographs of anthropogenic, biogenic, and geogenic components

(A) Heated bone (yellow-orange color in PPL) (scale bar, 250 µm), (B) fossiliferous limestone fragment (scale bar, 500 µm), (C) rodent tooth (scale bars, 500 µm), (D) shell fragment (scale bar, 500 µm), (E) accumulation of ash rhombs (marked by red arrow) (scale bar, 100 µm), (F) unburned mesofaunal excrements forming pellets (note orange color due to high organic content) around plant remains (scale bar, 500 µm), (G) charred mesofaunal excrements forming pellets embedded in the MB matrix (scale bar, 750 µm), (H) calcified plant pseudomorphs (marked by red arrow) (scale bar, 250 µm). PPL, plane-polarized light; XPL, cross-polarized light.

clearly outside the "gray area" (PSR = 1–5) defined by Gur-Arieh et al.[37] MW shows a value higher than 5, which is indicative of wood-dominated ash. On the other hand, MB and MR display values lower than 1, which indicates a predominant dung ash composition (Figure 7). The analysis of phytolith morphotypes indicates a dominance of monocotyledon over dicotyledon taxa both in EC3 and in the control sample (Figure 8). Identified morphotypes, taxonomic attribution, and their relative average abundance are listed in Table S2.

n-Alkanes

All three microunits show mid- and long-chain *n*-alkane (>nC_{21}) odd-over-even predominance ranging from nC_{23} to nC_{33} with a total *n*-alkane concentration of 9.06 µg/gds (µg/g of dry sample) and unimodal distributions. C_{max} has been detected at nC_{31} for MR (3.52 µg/gds) and at nC_{33} for MW (2.98 µg/gds) and MB (2.56 µg/gds). The control sample shows a C_{max} at nC_{31}, a carbon chain distribution from nC_{25} to nC_{35}, and a higher total concentration of 11.69 µg/gds (Figure 9; Table 3). Tree and shrub alkane maxima are commonly found in nC_{27} and nC_{29}, while grasses and herbs are dominated by nC_{31} and nC_{33}.[59] Because the composition and abundance of *n*-alkanes vary between plant species, tissues, and growth stages,[60,61] the distribution of *n*-alkanes was also evaluated using long-chain *n*-alkane ratios: $nC_{31}/(nC_{29} + nC_{31})$ and $nC_{31}/(nC_{27} + nC_{31})$ and $(nC_{31} + nC_{33})/(nC_{27} + nC_{29} + nC_{31} + nC_{33})$ aiming to determine the percentage contribution of grasses and herbs versus trees and shrubs to the total content of fossil plant alkanes in our samples.[62–64] The highest contribution of herbaceous vegetation (i.e., plants with flexible, green stems with few to no woody parts) occurs in the control sample (81.5%) and the lowest in MW and MB (54.8% and 54.3%, respectively) (Table 4).

Compound-specific stable carbon isotopes

We analyzed the carbon isotope ratios from alkanes nC_{27}, nC_{29}, nC_{31}, and nC_{33}. The isotopic composition for all samples falls into the range of C3 plants with a total range within −33.13‰ and −28.79‰ and a mean of −31.16‰ (Figure 10; Table 5). To further evaluate possible isotopic and molecular changes due to thermal alteration between samples, an ANOVA analysis was performed to compare the means of our groups of samples, showing no significant differences between them (p value = 0.8465). Additionally, a Tukey test was performed (MR-MB p value = 0.9216992, MW-MB p value = 0.8568542, MW-MR p value = 0.9880570). Overall, $\delta^{13}C$ values in our

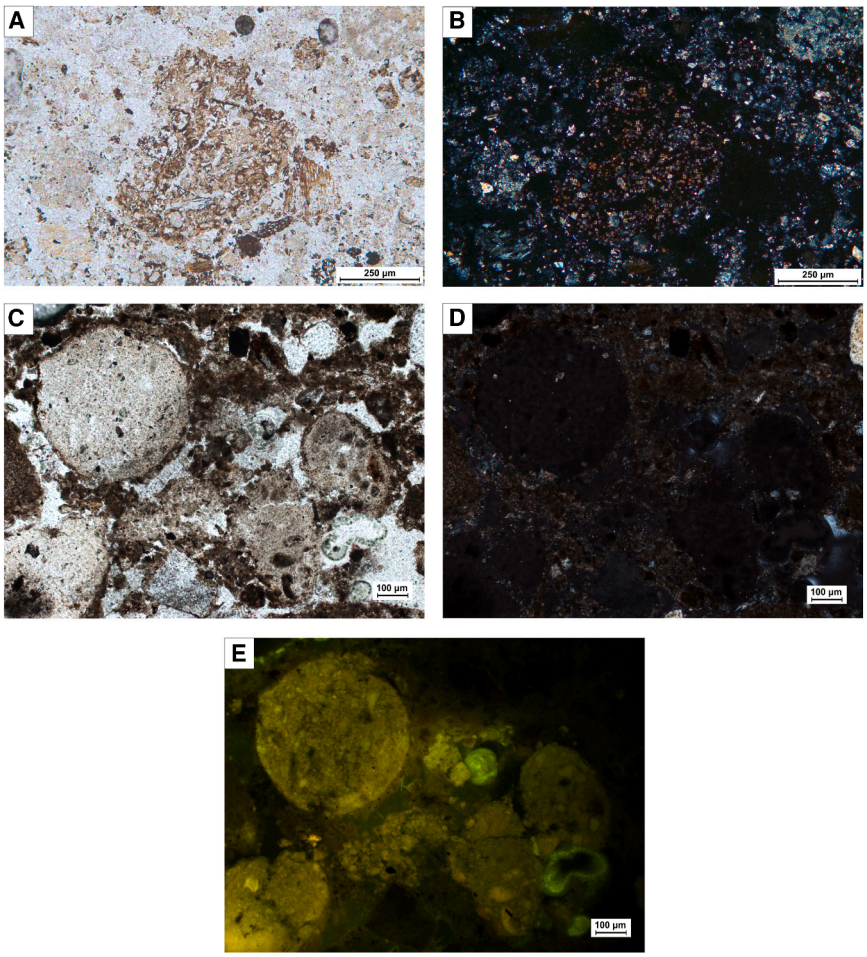

Figure 5. Micromorphological indicators of excrement

(A) Coprolite fragment (PPL) (scale bar, 250 μm); (B) same as (A) in XPL (note the abundant fecal spherulites inside) (scale bar, 250 μm); (C) phosphatic nodules (PPL) (note white-yellowish color) (scale bar, 100 μm); (D) same as (C) in XPL (scale bar, 100 μm); (E) same as (C) in BL (note how the nodules fluoresce) (scale bar, 100 μm). PPL, plane-polarized light; XPL, cross-polarized light; BL, blue light.

samples show no significant variation between archaeological microunits, with mean values for MW of −30.59‰, −31.07‰ for MB, and −30.72‰ for MR. Interestingly, the control sample shows the most depleted ^{13}C values of them all (range: −33.13‰ to −30.78‰ and a mean of −32.25‰).

Fecal biomarkers

Steroids found within the combustion structure and control sample are shown in Table 6. In general terms, 5β-stanols and bile acids, which are key to identifying the origin of the fecal matter, have not been well preserved in EC3. Only epi-5β-stigmastanol has been detected in MR. Cholesterol, stigmasterol, β-sitosterol, and 5α-stigmastanol were identified in MB and MR. MW shows no steroid preservation. Conversely, the control sample shows a higher concentration of fecal biomarkers compared to the archaeological samples.

DISCUSSION

Characterization of EC3

The analysis carried out on EC3 has confirmed the presence of anthropogenic components embedded in a mixed sedimentary calcitic matrix of burned herbivore dung, combusted plant residues, and wood ashes. The high quantities of fecal spherulites within the sedimentary matrix of EC3, along with the detection of epi-5β-stigmastanol in MR, strongly indicate that the fecal material is predominantly derived from ruminants. The microscopic and biomolecular evidence for dung is more prevalent in the basal red layer (MR) and charred black layer (MB) when compared to the upper white layer (MW) of the combustion feature. MW shows a decrease in dung microremains and an increase in wood-derived ashes, with these results also being in accordance with the *n*-alkane data, where MR and MB have the highest contributions of grasses/herbs. This suggests that the fuel employed for igniting the combustion feature likely consisted of wood, which generally shows a superior thermal efficiency compared to dung when utilized as a source of fuel.[36,38,65,66] However, several factors can influence the performance of a fire, particularly in open-air contexts, such as the rate of oxygen flow circulating through the fuel, through the underlying layer, and through the entire combustion structure itself.[67] The control sample, on the other hand, contains fecal spherulites and fecal biomarkers, probably related to wild and domestic roaming animals in the area, which is known to have recently supported modern pastoral activity.

The elevated abundance of phytoliths observed in microunits MR and MB, in contrast to MW and the control sample, is plausibly attributed to the increased deposition of dung rich in grasses. This association can be explained by the notably high silica content found in grasses, a characteristic feature that constitutes a primary mineral residue in animal dung.[67,68] Phytoliths are particularly abundant in grasses, resulting in phytolith concentration in grass ash being up to 20 times higher when compared with wood ash.[69] Thus, the phytolith assemblage in MR and MB seems to be directly linked with the plants used as fodder or forage consumed by the sheltered animals.

The phytolith morphotype analysis shows dominance of monocotyledon species in EC3 (see Figure 8), especially Poaceae (grasses) and Cyperaceae (sedges). However, we detect a slightly higher percentage of dicotyledon plants in MW

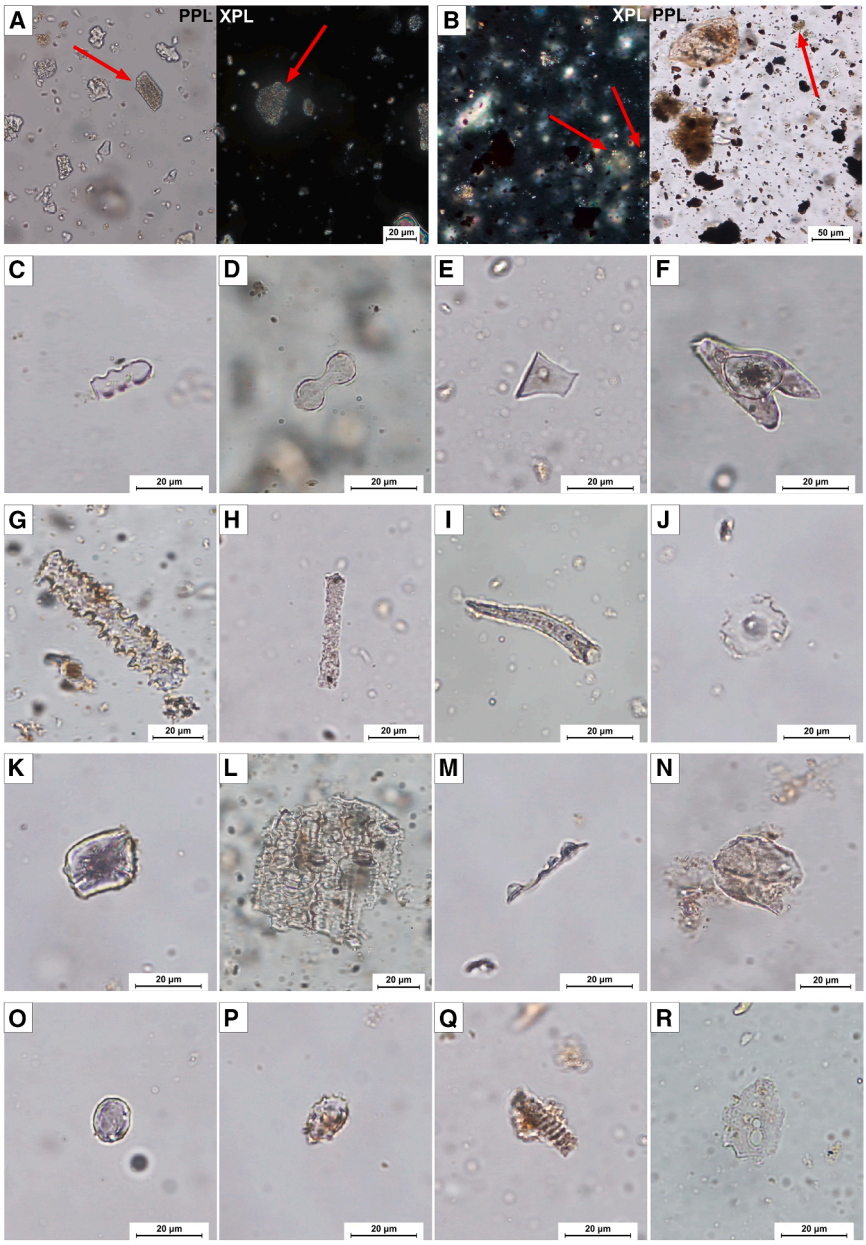

Figure 6. Selection of photomicrographs of calcitic microremains and phytoliths

(A) Ash pseudomorphs (scale bar, 20 µm), (B) fecal spherulites (scale bar, 50 µm), and (C–R) selected phytolith morphotypes (scale bars, 20 µm): (C) Crenate, (D) Bilobate, (E) Rondel, (F) Acute bulbosus, (G) Elongate dentate (weathered), (H) Elongate entire (highly weathered), (I) Acicular psilate, (J) Papillate, (K) Blocky psilate, (L) Elongate dentate/sinuate (multicell structure), (M) Hat-shaped, (N) Polyhedral facetate, (O) Spheroid psilate, (P) Ellipsoidal plicate, (Q) Tracheary annulate, (R) melted silica structure. PPL, plane-polarized light; XPL, cross-polarized light.

and the control sample. This is another indication of the use of woody fuel represented in MW, which adds to the results from the higher percentage contribution of trees and shrubs from fossil *n*-alkanes. The control sample, on the other hand, probably represents the local vegetation, which nowadays is characterized by a *Quercus rotundifolia* woodland with *Acer*

Table 2. Estimated amounts of fecal spherulites, ash pseudomorphs, and phytoliths per gram of sediment in EC3 and control samples

Sample	Estimated amount of fecal spherulites per gram of sediment	Estimated amount of ash pseudomorphs per gram of sediment	PSR value	Estimated amount of phytoliths per gram of burned sediment	No. of morphotypes identified	Percentage of weathered morphotypes	% melted phytoliths
MW	461,410	3,765,698	8.16	982,648	252	19.5	3
MB	2,986,211	2,213,659	0.74	2,042,860	264	17.5	1
MR	5,675,816	4,540,653	0.8	2,421,741	273	14.5	1.5
Control	559,406	0	0	734,805	256	5	–

Values for the pseudomorphs-spherulites ratio (PSR) are also indicated, as well as the number of identified phytolith morphotypes. The proportion of weathered and melted phytoliths has been calculated over an assemblage of 200 morphotypes.

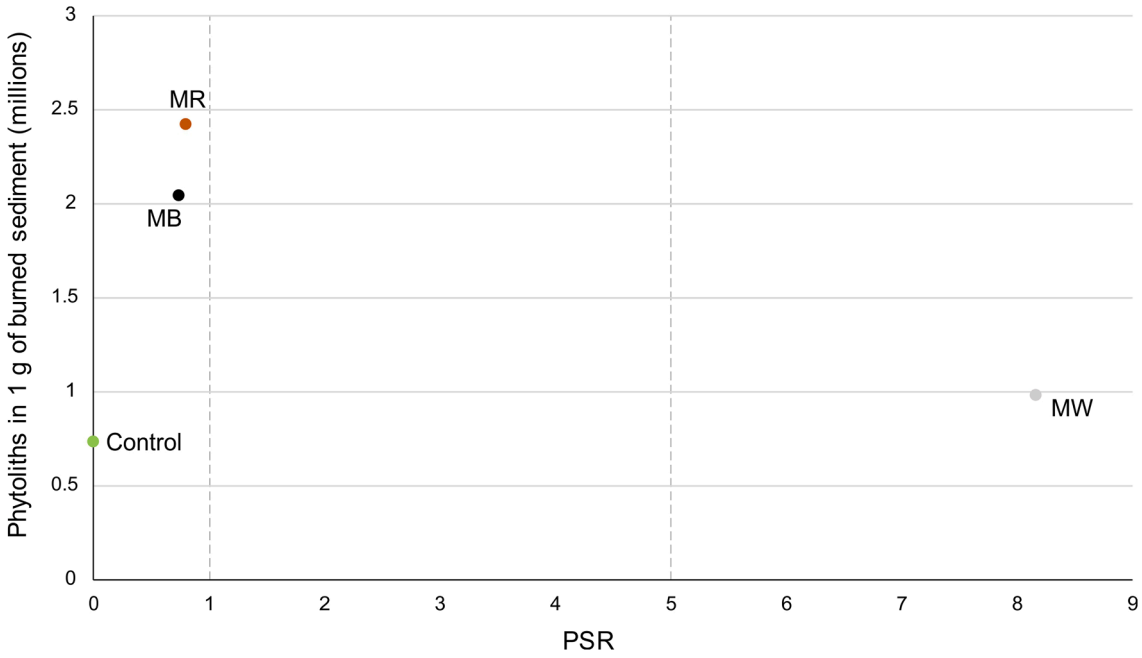

Figure 7. EC3 and control samples plotted by PSR (*x* axis) against phytolith abundance in 1 g of burned sediment (*y* axis)
Dashed lines indicate PSR limits established by Gur-Arieh et al.[37] for dung ash (<1), gray area (1–5), and wood ash (>5).

monspessulanum and *Pinus sylvestris*. At lower elevations of southern locations, a mixed oak forest (*Quercus rotundifolia* and *Q. pubescens*) is present.[70] There is no indication of conifer species in the molecular signature from the archaeological samples, with dehydroabietic acid (RT 33.37, Match 655, R-Match 691; identified with injected standard; a biomarker for conifer

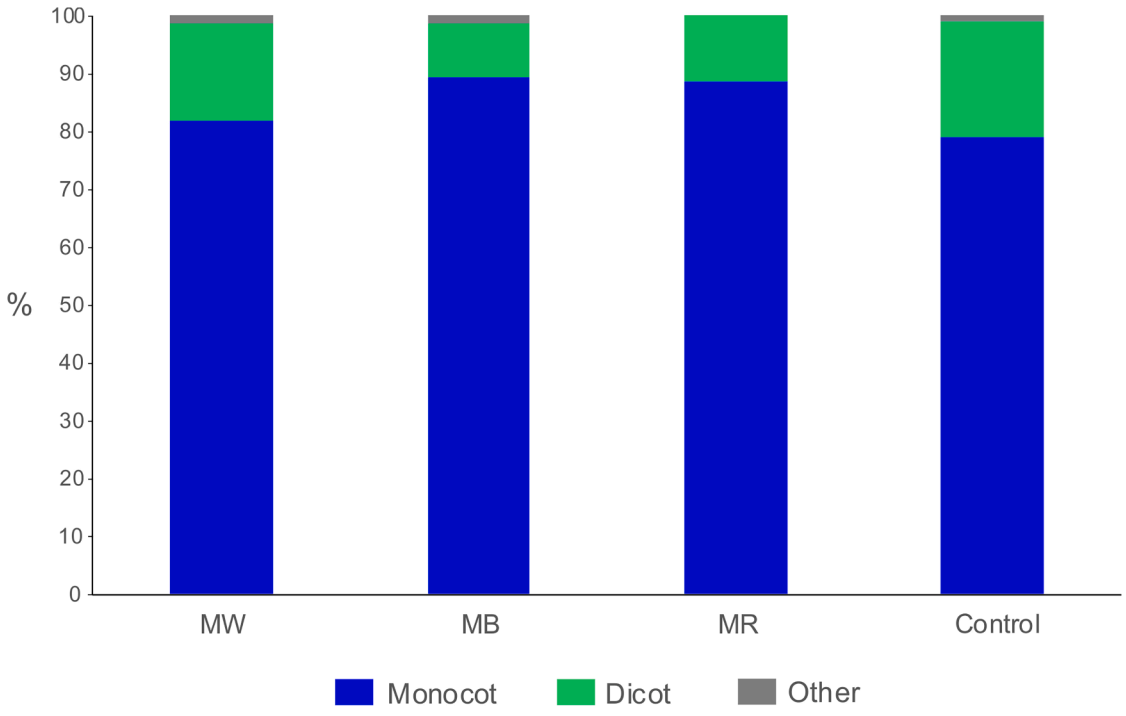

Figure 8. Relative abundance of monocotyledon vs. dicotyledon phytolith morphotypes based on the assemblage recovered from EC3 and the control sample

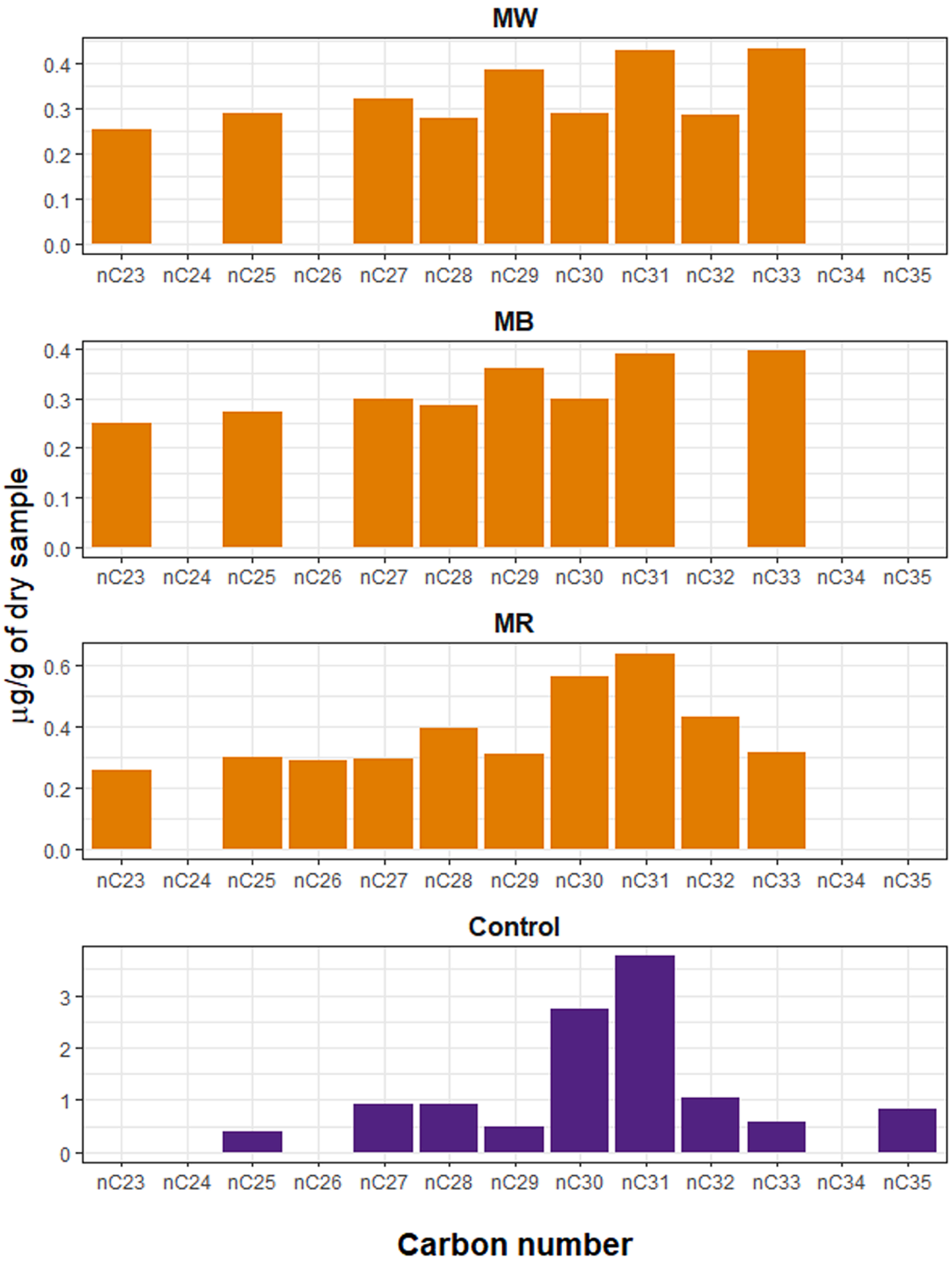

Figure 9. Bar plots indicating the distribution and concentration of *n*-alkanes in sediments from archaeological (orange) and control (purple) samples

C_{max} is nC_{31} for MR and the control sample, while nC_{33} is the peak maximum carbon number for MW and MB. The concentrations are given in µg/g of dry sample. Note that the *y* axis is in variable scale.

Table 3. *n*-Alkane concentration (μg/g of dry sample), including total and mean values, for each sample collected from EC3 and the control sample

Sample	Total	Mean	nC_{23}	nC_{25}	nC_{26}	nC_{27}	nC_{28}	nC_{29}	nC_{30}	nC_{31}	nC_{32}	nC_{33}	nC_{35}
MW	2.98	0.27	0.26	0.29	0.00	0.32	0.28	0.39	0.29	0.43	0.29	0.43	0.00
MB	2.56	0.23	0.25	0.27	0.00	0.30	0.29	0.36	0.30	0.39	0.00	0.40	0.00
MR	3.52	0.31	0.26	0.30	0.29	0.30	0.39	0.31	0.57	0.64	0.43	0.02	0.00
Control	11.69	1.06	0.00	0.41	0.00	0.91	0.91	0.49	2.74	3.76	1.05	0.58	0.84

resin according to Simoneit et al.[71]) only found in the control sample. We also calculated the abundance of inflorescences compared to leaves/stems phytoliths. Inflorescences appear to be higher in MB (~44%) and MR (~31%) in comparison with MW (~23%) and control (~14%) (Figure S2). Since MB and MR are mostly composed of dung, we suspect that the input of inflorescences is related to the plants directly consumed by the animals kept at Xicotó. Moreover, the concentration of the nC_{27} *n*-alkane, which is generally related to seeds and mature plants[72] together with shrubby vegetation, is relatively low in the control sample, which was collected in late March. This could indicate that the moment of consumption of young plants would be during early summer in a free-range consumption or in any other moment if the animals were provided with fodder that was collected around that season when plants would be producing early seeds and having mature inflorescences. In addition, the observed variation in the $\delta^{13}C$ isotope values between archaeological samples and the control sample might signify shifts in environmental conditions, as the carbon isotopic fractionation in plants correlates with average yearly precipitation and temperature,[73] but it also could be a reflection of the influence of thermal alteration, where above 250°C and 350°C there is an increment of 2‰–4‰ in the $\delta^{13}C$ values related to the selective release of ^{12}C-enriched CO_2 from organic matter during heating.[74,75] Future referential studies on the local vegetation are needed to address questions surrounding seasonality.

Comparison to *fumier* deposits

The abundance of fecal spherulites in *fumiers* contexts is extremely varied, not only between the different layers within the same sequence but also between sites. Amounts can vary from less than 1 million up to 1,000 million spherulites per gram of sediment.[76] Some average values of fecal spherulite abundance per sample collected in *fumier* deposits in the Iberian Peninsula—without taking into account the degree of thermal alteration and preservation of the sampled layers—are gathered here: Neolithic-Bronze Age levels of Cova Gran de Santa Linya (Lleida, Spain), for example, show high values of up to 90 million spherulites per gram of sediment in average.[77] Around 6.9 million spherulites per gram of sediment have been detected in an average sample in Los Husos II (Álava, Spain) north profile[40] and around 4 million spherulites in its south-eastern profile, both dating to the Neolithic.[39] Neolithic levels of San Cristóbal (Álava, Spain) *fumier* deposits indicate amounts of 1.3–4 million spherulites per gram of sediment, while El Mirador (Burgos, Spain) shows an important variability, averaging 2.1 million fecal spherulites across its *fumier* sequence dating to the Late Neolithic (MIR6)[40] and ca. 676 million in its Bronze Age sequence (MIR104-105).[76] Xicotó EC3 values average around 3 million spherulites per gram of sediment and are thus comparable to the average values of samples gathered from Neolithic *fumiers*, suggesting a significant accumulation of dung in this particular area of the rockshelter. In spite of observing the darkening process in many fecal spherulites, which occurs due to an exposure to burning temperatures of ca. 500°C–700°C,[58,78] it is possible that temperatures might not have surpassed 700°C in EC3, above which spherulites start disappearing. This could be a reason why a high number of these calcitic microremains have been preserved. This is consistent with the low amount of melted phytoliths (melting usually occurring at 800°C–900°C[37,78]) detected in the combustion feature (see Table 2).

Phytolith abundance, however, is on average higher in samples of these *fumier* contexts compared to Xicotó, displaying average amounts of ca. 6 - 8 million phytoliths per g of sediment (San Cristóbal), 16 million (El Mirador, MIR6), and 5.5 - 13 million phytoliths (Los Husos II).[39,40] Xicotó average does not surpass the 1.9 million phytoliths per g of sediment. We would expect that the number of animals sheltered in the reduced space of Xicotó rockshelter was lower compared to other bigger cave contexts, which could explain the lower phytolith concentrations. Alternatively, this could be related to the differential phytolith-productive plant input, as well as different degrees of preservation.

Preservation and thermal degradation

The biomolecular signal in EC3 shows differential preservation, most likely related to the thermal degradation effect on the

Table 4. *n*-Alkane ratio values for EC3 and control samples (in %) and mean

Sample	$nC_{31}/nC_{27} + nC_{31}$	$nC_{31}/nC_{29} + nC_{31}$	$nC_{31} + nC_{33}/nC_{27} + nC_{29} + nC_{31} + nC_{33}$	Mean
MW	57.3	52.4	54.8	54.8
MB	56.5	52	54.5	54.3
MR	68.1	67.4	52	62.5
Control	80.5	88.5	75.6	81.5

Aimed at determining the percentage contribution of grasses and herbs versus trees and shrubs to the total content of fossil plant alkanes.

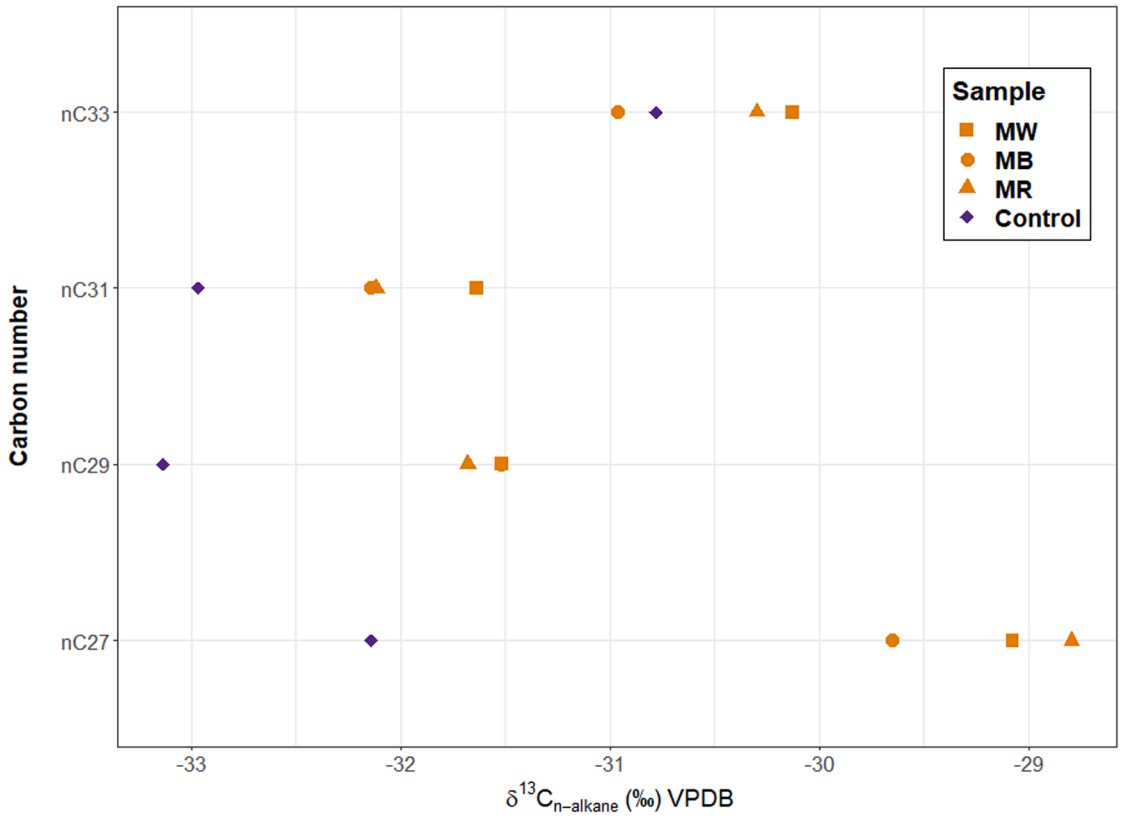

Figure 10. Carbon isotope compositions of *n*-alkanes from MW, MB, MR (orange), and control (purple) samples
The isotopic composition for all samples falls into the range of C3 plants with a range within −33.13‰ and −28.79‰ and a mean of −31.16‰.

biomarkers. In the case of MW, the absence of preserved steroid compounds is evident, suggesting the likelihood of experiencing the most elevated burning temperatures. In MR, although expected to be less thermally altered, it is possible that the temperature could be high enough for these compounds to disappear. *n*-Alkane concentration in MW is however similar to MB (see Figure 9). We also notice a decrease in the concentration of *n*-alkanes and steroids in EC3 compared to the control sample (i.e., non-burned natural sediment) (see Figure 9; Table 6), possibly related to the temperatures reached, as they start to strongly degrade above 450°C.[79] The isotopic signatures show on average $\delta^{13}C$ more positive values than those from the control sample, which might be an indication of thermal alteration. Previous studies have shown that with increasing temperatures, there is a shift to more enriched $\delta^{13}C$ values,[80] this pattern being even more evidenced in charred leaves than in bark remains.[81]

Functionality of EC3

Understanding the function of fire is key to characterize the past occupation and use of space at Xicotó. From a micromorphological view, we observe *in situ* burning features in MR despite the evident mesofaunal reworking of the lower layers, which might have translocated ashes originally deposited in MW. Therefore, we suspect that the deposited dung in MR and MB seems to have been intentionally burned after its accumulation in this area of the rockshelter. The rate of dung accumulation is uncertain, but we detect a significant amount of dung microremains when compared to other archaeological stabling deposits from similar chronologies. Some animals, most likely ruminants, were sheltered during the Neolithic occupation of the rockshelter. However, unlike the known and well-studied *fumier* sequences dating to this period,[12,14] EC3 represents a single and localized dung combustion event, which could be the consequence of a rather sporadic presence of livestock at Xicotó.

Table 5. Carbon stable isotope ($\delta^{13}C$) values (in ‰) and mean (± standard deviation) of *n*-alkanes from EC3 samples and the control sample

Sample	nC_{27}	nC_{29}	nC_{31}	nC_{33}	Mean
MW ± SD	−29.08 ± 0.22	−31.51 ± 0.09	−31.64 ± 0.03	−30.13 ± 0.49	−30.59
MB ± SD	−29.65 ± 0.06	−31.51 ± 0.12	−32.14 ± 0.11	−30.90 ± 0.23	−31.07
MR ± SD	−28.79 ± 0.19	−31.68 ± 0.24	−32.11 ± 0.10	−30.30 ± 0.09	−30.72
Control ± SD	−32.14 ± 0.15	−33.13 ± 0.04	−32.97 ± 0.11	−30.78 ± 0.16	−32.25

Table 6. Calculated concentrations (± uncertainty) (μg/g of dry sample) of targeted steroids

Sample	Copr	Epicopr	Cholest	5α-Cholest	5β-Stigm	Epi-Stigm	Stigste	β-Sito	5α-Stigm	LCA	DCA	CDCA	HDCA	UDCA
MW	ND	ND	ND	ND	ND	ND	ND	ND	ND	ND	ND	ND	ND	ND
MB	ND	ND	$1.08 \cdot 10^{-1} \pm 0.00{\cdot}10^{-1}$	ND	ND	ND	$1.07 \cdot 10^{-1} \pm 0.00{\cdot}10^{-1}$	$9.23 \cdot 10^{-1} \pm 0.00{\cdot}10^{-1}$	$0.18 \cdot 10^{-1} \pm 0.00{\cdot}10^{-1}$	ND	ND	ND	ND	ND
MR	ND	ND	$0.91 \cdot 10^{-1} \pm 0.00{\cdot}10^{-1}$	ND	< LOQ	$0.53 \cdot 10^{-1} \pm 0.00{\cdot}10^{-1}$	$0.63 \cdot 10^{-1} \pm 0.00{\cdot}10^{-1}$	$3.12 \cdot 10^{-1} \pm 0.00{\cdot}10^{-1}$	$0.05 \cdot 10^{-1} \pm 0.00{\cdot}10^{-1}$	ND	ND	ND	ND	ND
Control	ND	ND	$3.80 \cdot 10^{-1} \pm 0.00{\cdot}10^{-1}$	$0.53 \cdot 10^{-1} \pm 0.00{\cdot}10^{-1}$	$4.22 \cdot 10^{-1} \pm 0.00{\cdot}10^{-1}$	$2.73 \cdot 10^{-1} \pm 0.00{\cdot}10^{-1}$	$4.08 \cdot 10^{-1} \pm 0.00{\cdot}10^{-1}$	$22.04 \cdot 10^{-1} \pm 0.00{\cdot}10^{-1}$	$4.98 \cdot 10^{-1} \pm 0.00{\cdot}10^{-1}$	< LOQ	$0.01 \cdot 10^{-1} \pm 0.00 \cdot 10^{-1}$	ND	ND	ND

Copr, coprostanol; Epicopr, epicoprostanol; Cholest, cholesterol; 5α-Cholest, 5α-cholestanol; 5β-Stigm, 5β-stigmastanol; Epi-Stigm, epi-5β-stigmastanol; Stigste, stigmasterol; β-Sito, β-sitosterol; 5α-Stigm, 5α-stigmastanol; LCA, lithocholic acid; DCA, deoxycholic acid; CDCA, chenodeoxycholic acid; HDCA, hyodeoxycholic acid; UDCA, ursodeoxycholic acid; ND, not detected; LOQ, limit of quantification.

Final remarks

Compelling evidence of ruminant dung suggests that animals sought shelter at Abric del Xicotó, possibly during late spring or early summer, according to phytolith and isotopic data. Additionally, the combustion structure appears to have been utilized at least once, maybe for cleaning or heating purposes, with wood being used as the primary fuel. This new data can significantly enhance the investigation of the first pastoralist Neolithic groups in eastern Iberia by providing a more comprehensive and nuanced understanding of their lifestyles, activities, food sources, and interactions with the environment. Moreover, it can be compared with data from other Neolithic sites within eastern Iberia and neighboring regions. This comparative approach allows the identification of commonalities, differences, and potential cultural exchanges between different groups.

Finally, it is also important to highlight that carrying out a multiproxy approach has allowed us to identify dung at the microscale across all samples but only in one sample at the molecular scale due to poor fecal lipid biomarker preservation states. In this case, the abundance of excremental microremains has been key to detect fecal input in the combustion feature.

Limitations of the study

We have only studied a single combustion structure comprising three archaeological samples, making the application of multivariate statistical techniques challenging due to the limited scope of our dataset. Further assessment of other areas of Xicotó rockshelter showing combustion residues, as well as areas showing no combustion, is needed in order to fully understand the use of space and human activities carried out during its prehistoric occupation.

RESOURCE AVAILABILITY

Lead contact

Further information and requests should be directed to and will be fulfilled by the lead contact, Natalia Égüez (natalia.eguez@ipna.csic.es).

Materials availability

This study did not generate new reagents or materials.

Data and code availability

- R dataset files for reproducibility can be found in the GitHub repository: https://github.com/Neguez/2025-Xicoto.git. The rest of the data reported in this paper will be shared by the lead contact upon request.
- All original code has been deposited at https://github.com/Neguez/2025-Xicoto.git and is publicly available as of the date of publication (https://doi.org/10.5281/zenodo.15756264).
- Any additional information required to reanalyze the data reported in this paper is available from the lead contact upon request.

ACKNOWLEDGMENTS

The research leading to these results has received funding from the Spanish Ministry of Science, Innovation and Universities FPU predoctoral contract (E.F.-P., no. FPU2019-02379), the MSCA-IF-2020 programme (N.E., no. 101032608), and the Ramón y Cajal programme (N.E., no. RYC2022-036901-I, MCIN/AEI/10.13039/501100011033 and FSE+). Archaeological works at Abric del Xicotó have been supported by the University of Barcelona and projects CLT009/18/00030, CLT009/22/00076, and SGR2021-00337 from the Catalan Government. The radiocarbon dates were financially supported by the Spanish project PID2020-113960GB-I00 and projects "The chronology of the Prehistory in NE Iberia" and "Analytical study of the human prehistoric sequence in the

middle and upper Segre river" from the PALARQ Foundation. We thank Shira Gur-Arieh for her support during the analysis of microremains.

AUTHOR CONTRIBUTIONS

E.F.-P.: conceptualization, validation, investigation, formal analysis, writing – original draft preparation, and visualization; N.E.: conceptualization, software, validation, investigation, formal analysis, visualization, writing – review and editing, and supervision; C.G.-O.: resources, writing – review and editing, and project administration; A.V.H.-H.: methodology, validation, writing – review and editing, and supervision; C.M.: resources, writing – review and editing, and supervision; X.M.: conceptualization, resources, writing – review and editing, project administration, and funding acquisition; M.S.d.l.T.: conceptualization, resources, writing – review and editing, project administration, and funding acquisition.

DECLARATION OF INTERESTS

The authors acknowledge that C.M. is the guest editor for the special issue "Advances in Biomolecular Archaeology and Forensic Sciences" but was not involved in the editorial handling of this article.

DECLARATION OF GENERATIVE AI AND AI-ASSISTED TECHNOLOGIES IN THE WRITING PROCESS

During the preparation of this work, the authors used ChatGPT in order to improve the language and readability of the manuscript. After using this tool, the authors reviewed and edited the content as needed and take full responsibility for the content of the publication.

STAR★METHODS

Detailed methods are provided in the online version of this paper and include the following:

- KEY RESOURCES TABLE
- EXPERIMENTAL MODEL AND SUBJECT DETAILS
- METHOD DETAILS
  - Soil micromorphological analysis
  - Analysis of calcitic and siliceous microremains: Fecal spherulites, ash pseudomorphs and phytoliths
  - Biomarker analysis
  - Instrumental analysis
  - Compound-specific stable carbon isotopes
  - Data visualization
- QUANTIFICATION AND STATISTICAL ANALYSIS
  - Microremains
  - Biomarkers
  - Statistical analysis

SUPPLEMENTAL INFORMATION

Supplemental information can be found online at https://doi.org/10.1016/j.isci.2025.113293.

Received: October 10, 2023
Revised: March 19, 2024
Accepted: July 31, 2025
Published: August 7, 2025

REFERENCES

1. Zapata, L., Peña-Chocarro, L., Pérez-Jordà, G., and Stika, H. (2004). Early Neolithic agriculture in the Iberian Peninsula. World Archaeol. *18*, 283–325. https://link.springer.com/article/10.1007/s10963-004-5621-4.
2. de Lagrán, Í.G.M. (2015). Recent data and approaches on the Neolithization of the Iberian Peninsula. Eur. J. Archaeol. *18*, 429–453. https://doi.org/10.1179/1461957114Y.0000000084.
3. Szécsényi-Nagy, A., Roth, C., Brandt, G., Rihuete-Herrada, C., Tejedor-Rodríguez, C., Held, P., García-Martínez-de-Lagrán, Í., Arcusa Magallón, H., Zesch, S., Knipper, C., et al. (2017). The maternal genetic make-up of the Iberian Peninsula between the Neolithic and the Early Bronze Age. Sci. Rep. *7*, 15644. https://www.nature.com/articles/s41598-017-15480-9.
4. Revelles, J., Burjachs, F., Palomo, A., Piqué, R., Iriarte, E., Pérez-Obiol, R., and Terradas, X. (2018). Human-environment interaction during the Mesolithic-Neolithic transition in the NE Iberian Peninsula. Vegetation history, climate change and human impact during the Early-Middle Holocene in the Eastern Pre-Pyrenees. Quat. Sci. Rev. *184*, 183–200. https://doi.org/10.1016/j.quascirev.2017.08.025.
5. Oms, F.X. (2014). La neolitització del nord-est de la Península Ibèrica a partir de les datacions radiocarbòniques i les primeres ceràmiques impreses c. 5600-4900 cal BC (Universitat de Barcelona). PhD Thesis.
6. Oms, F.X., Sánchez de la Torre, M., Petit, M.A., López-Cahero, F.J., and Mangado, X. (2019). Nuevos datos del VI y V milenio cal BC en el llano y Prepirineo de Lleida (NE de la Península Ibérica): el Abric del Xicotó y Lers Auvelles. MUNIBE Antropologia-Arkeologia *70*, 93–107.
7. Cámara Manzaneda, J., Clop García, X., García Rosselló, J., and Martín Cólliga, A. (2022). Pottery forming of the Cardial and Epicardial Neolithic wares: Analysis and systematisation of technological traces from the ceramic productions of Cova del Frare (NE Iberian Peninsula, 5200-4800 BCE). J. Archaeol. Sci. Reports *43*, 103457. https://doi.org/10.1016/j.jasrep.2022.103457.
8. Gassiot, E., Rodríguez, D., Pèlachs, A., Pérez, R., Julià, R., Bal-Serin, M.C., and Mazzucco, N. (2014). La alta montaña durante la Prehistoria. 10 años de investigación en el Pirineo catalán Occidental. Trabajos Prehist *71*, 261–281.
9. Palet, J.M., Orengo, H.A., García, A., Polonio, T., Ejarque, A., Miras, Y., and Riera, S. (2022). Landscape archaeology in eastern Pyrenees high mountain areas (Segre & Ter valleys): human activities in the shaping of Mountain Cultural landscapes. In Archaeology of Mountain Landscapes: Interdisciplinary Research Strategies of Agro-Pastoralism in Upland Regions, M. García-Molsosa, ed. (State University of New York Press), pp. 179–196.
10. Gassiot, E., Mazzucco, N., Obea, L., Tarifa, N., Antolín, F., Clop, X., Navarrete, V., and Saña i Seguí, M. (2015). La Cova del Sardo de Boí i l'explotació de l'alta muntanya als Pirineus occidentals en època neolítica. Tribuna d'Arqueologia *2012–2013*, 199–218.
11. Tejedor-Rodríguez, C., Moreno-García, M., Tornero, C., Hoffmann, A., García-Martínez, I., Arcusa-Magallón, H., Garrido-Pena, A., Royo-Guillén, J.-I., Díaz-Navarro, S., Peña-Chocarro, L., et al. (2020). Investigating neolithic caprine husbandry in the central Pyrenees: insights from a multi-proxy study at Els Trocs cave (Bisaurri, Spain). PLoS One *16*, e0244139. https://doi.org/10.1371/journal.pone.0244139.
12. Martín, P., and Oms, F.X. (2021). Early Neolithic Husbandry in the Pre-Pyrenean Area. The Management of Herds at the Cova Colomera (Serra del Montsec, Spain) and its Implications for the Early Occupation of the Region. Open Archaeol. *7*, 1216–1234. https://doi.org/10.1515/opar-2020-0190.
13. Polo-Díaz, A., Martínez-Moreno, J., Benito-Calvo, A., and Mora, R. (2014). Prehistoric herding facilities: site formation processes and archaeological dynamics in Cova Gran de Santa Linya (Southeastern Prepyrenees, Iberia). J. Archaeol. Sci. *41*, 784–800. https://doi.org/10.1016/j.jas.2013.09.013.
14. Bergadà, M.M., and Oms, F.X. (2021). Pastoral Practices, Bedding and Fodder During the Early Neolithic Through Micromorphology at Cova Colomera (Southeastern Pre-Pyrenees, Iberia). Open Archaeol. *7*, 1258–1273. https://doi.org/10.1515/opar-2020-0183.
15. Oms, X., Bargalló, A., Chaler, M., Fontanals, M., García, M.S., López-García, J.M., Morales, J.I., Nievas, T., Rodríguez, A., Serra, J., et al. (2008). La

Cova Colomera (Sant Esteve de la Sarga, Lleida), una cueva-redil en el Prepirineo de Lérida. Primeros resultados y perspectivas de futuro. IV Congreso del Neolítico de la Península Ibérica *1*, 230–237. https://www.academia.edu/download/7278696/Colomera_Congres%20Alacant.pdf.

16. Mora, R., Benito-Calvo, A., Martínez-Moreno, J., Marcen, P.G., and de La Torre, I. (2011). Chrono-stratigraphy of the Upper Pleistocene and Holocene archaeological sequence in Cova Gran (south-eastern Pre-Pyrenees, Iberian Peninsula). J. Quaternary Sci. *26*, 635–644. https://doi.org/10.1002/jqs.1486.
17. Utrilla, P., and Laborda, R. (2018). La cueva de Chaves (Bastarás, Huesca): 15 000 anos de ocupación prehistórica. Trabajos Prehist *75*, 248–269. https://doi.org/10.3989/tp.2018.12214.
18. Daura, J., Sanz, M., Oms, F.X., Pedro, M., Martínez, P., Mendiela, S., Oliva Poveda, M., Gibaja, J.F., Mozota, M., Alonso-Eguíluz, M., et al. (2019). Deciphering Neolithic activities from a Cardial burial site (Cova Bonica) on the western Mediterranean coast. J. Archaeol. Sci. Reports *23*, 324–347. https://doi.org/10.1016/j.jasrep.2018.10.036.
19. Antolín, F., Martínez, P., Fierro-Milà, E., León, M., Martínez, H., Gascón, M., Bergadà, M., Prats, G., Barceló, J.A., and Edo, M. (2016). Towards the periodization of the uses of Can Sadurní Cave (Begues, Catalonia) during the Middle Neolithic I. The contribution of Bayesian modelling to radiocarbon dating sequences. In Actas del Congreso de Cronometrías para La Historia de La Península Ibérica, pp. 55–66.
20. Bergadà, M.M., Cervelló, J.M., Edo, M., and Antolín, F. (2018). Depositional and anthropic processes in the Holocene record of the Can Sadurní cave (Begues, Barcelona, Spain): microstratigraphic contributions. Bol. Geol. Min. *129*, 251–284. https://inis.iaea.org/search/search.aspx?orig_q=RN:49090545.
21. Lancelotti, C., Balbo, A.L., Madella, M., Iriarte, E., Rojo-Guerra, M., Royo, J.I., Tejedor, C., Garrido, R., García, I., Arcusa, H., et al. (2014). The missing crop: investigating the use of grasses at Els Trocs, a Neolithic cave site in the Pyrenees (1564 m asl). J. Archaeol. Sci. *42*, 456–466. https://doi.org/10.1016/j.jas.2013.11.021.
22. Clemente-Conte, I., Gassiot Ballbè, E., Lanaspa, J.R., Mazzucco, N., and Gómez, L.O. (2014). "Cort o Transito" -Coro Trasito- o corral de tránsito: una cueva pastoril del Neolítico antiguo en el corazón de Sobrarbe. In Sobrarbe antes de Sobrarbe. Pinceladas de historia de los Pirineos, I. Clemente Conte, G. Ballbè, and J. Rey Lanaspa, eds. (Instituto de Estudios Altoaragoneses), pp. 11–32.
23. Clemente-Conte, I., Gassiot Ballbé, E., Rey Lanaspa, J., Antolín Tutusaus, F., Obea Gómez, L., Viñerta Crespo, A., and Saña Seguí, M. (2016). Cueva de Coro Trasito (Tella-Sin, Huesca): un asentamiento pastoril en el Pirineo central con ocupaciones del Neolítico Antiguo y del Bronce Medio. II Congreso CAPA. In Arqueología y Patrimonio Aragonés, (Colegio Oficial de Doctores y Licenciados en Filosofía y Letras y en Ciencias de Aragón), pp. 75–84.
24. M.A. Petit, ed. El procés de neo-lititització a la vall del Segre: La cova del Parco (Alòs de Balaguer, la Noguera): Estudi de lesocupacions humanes del v al ii mil·lenni aC. Monografies del SERP (Barcelona), *1*, pp. 1–69.
25. Oms, F.X., Martín, A., Esteve, X., Mestres, J., Morell, B., Subirà, M.E., and Gibaja, J.F. (2016). The Neolithic in Northeast Iberia: Chronocultural Phases and ^{14}C. Radiocarbon *58*, 291–309. https://doi.org/10.1017/RDC.2015.14.
26. Angelucci, D.E., Boschian, G., Fontanals, M., Pedrotti, A., and Vergès, J.M. (2009). Shepherds and karst: the use of caves and rock-shelters in the Mediterranean region during the Neolithic. World Archaeol. *41*, 191–214. https://doi.org/10.1080/00438240902843659.
27. Égüez, N., Mallol, C., Martín-Socas, D., and Cámalich, M.D. (2016). Radiometric dates and micromorphological evidence for synchronous domestic activity and sheep penning in a Neolithic cave: Cueva de El Toro (Málaga, Antequera, Spain). Archaeol. Anthrop. Sci. *8*, 107–123. https://doi.org/10.1007/s12520-014-0217-0.
28. Fernández-Palacios, E., Jambrina-Enríquez, M., Mentzer, S.M., Rodríguez de Vera, C., Dinckal, A., Égüez, N., Herrera-Herrera, A.V., Navarro Mederos, J.F., Marrero Salas, E., Miller, C.E., and Mallol, C. (2023). Reconstructing formation processes at the Canary Islands indigenous site of Belmaco Cave (La Palma, Spain) through a multiproxy geoarchaeological approach. Geoarchaeology *38*, 713–739. https://doi.org/10.1002/gea.21972.
29. Polo-Díaz, A., Alonso-Eguíluz, M., Ruiz, M., Pérez, S., Mújika, J., Albert, R.M., and Fernández Eraso, J. (2016). Management of residues and natural resources at San Cristóbal rock-shelter: Contribution to the characterisation of chalcolithic agropastoral groups in the Iberian Peninsula. Quatern. Int. *414*, 202–225. https://doi.org/10.1016/j.quaint.2016.02.013.
30. Brönnimann, D., Ismail-Meyer, K., Rentzel, P., Pümpin, C., and Lisá, L. (2017). Excrements of herbivores. In Archaeological Soil and Sediment Micromorphology, C. Nicosia and G. Stoops, eds. (Wiley-Blackwell), pp. 55–66.
31. Polo Díaz, A., and Fernández Eraso, J. (2010). Same anthropogenic activity, different taphonomic processes: A comparison of deposits from Los Husos I & II (Upper Ebro Basin, Spain). Quatern. Int. *214*, 82–97. https://doi.org/10.1016/j.quaint.2009.10.022.
32. Shahack-Gross, R. (2011). Herbivorous livestock dung: formation, taphonomy, methods for identification, and archaeological significance. J. Archaeol. Sci. *38*, 205–218. https://doi.org/10.1016/j.jas.2010.09.019.
33. Dunseth, Z.C., Junge, A., Fuchs, M., Finkelstein, I., and Shahack-Gross, R. (2016). Geoarchaeological investigation at the intermediate Bronze Age Negev highlands site of Mashabe Sade. Tel Aviv *43*, 43–75.
34. Dunseth, Z.C., Finkelstein, I., and Shahack-Gross, R. (2018). Intermediate Bronze Age subsistence practices in the Negev Highlands, Israel: Macro- and microarchaeological results from the sites of Ein Ziq and Nahal Boqer 66. J. Archaeol. Sci. Reports *19*, 712–726. https://doi.org/10.1016/j.jasrep.2018.03.025.
35. Eliyahu-Behar, A., Shai, I., Gur-Arieh, S., Frumin, S., Albaz, S., Weiss, E., Manclossi, F., Rosen, S., Greenfield, T.L., Greenfield, H.J., and Maeir, A.M. (2017). Early Bronze Age pebble installations from Tell es-Safi/Gath, Israel: evidence for their function and utilization. Levant *49*, 46–63. https://doi.org/10.1080/00758914.2017.1279495.
36. Gur-Arieh, S., Mintz, E., Boaretto, E., and Shahack-Gross, R. (2013). An ethnoarchaeological study of cooking installations in rural Uzbekistan: development of a new method for identification of fuel sources. J. Archaeol. Sci. *40*, 4331–4347. https://doi.org/10.1016/j.jas.2013.06.001.
37. Gur-Arieh, S., Shahack-Gross, R., Maeir, A.M., Lehmann, G., Hitchcock, L.A., and Boaretto, E. (2014). The taphonomy and preservation of wood and dung ashes found in archaeological cooking installations: case studies from Iron Age Israel. J. Archaeol. Sci. *46*, 50–67. https://doi.org/10.1016/j.jas.2014.03.011.
38. Portillo, M., Belarte, M.C., Ramon, J., Kallala, N., Sanmartí, J., and Albert, R.M. (2017). An ethnoarchaeological study of livestock dung fuels from cooking installations in northern Tunisia. Quat. Int. *431*, 131–144. https://doi.org/10.1016/j.quaint.2015.12.040.
39. Alonso-Eguíluz, M., Fernández-Eraso, J., and Albert, R.M. (2017). The first herders in the upper Ebro basin at Los Husos II (Álava, Spain): microarchaeology applied to fumier deposits. Veg. His. Archaeobot. *26*, 143–157. https://doi.org/10.1007/s00334-016-0590-y.
40. Alonso-Eguiluz, M., Albert, R.M., Vergès, J.M., and Fernández-Eraso, J. (2023). New insights into shepherds' activities: Multi-proxy approach applied to fumier deposits from the north of Iberian Peninsula. Quatern. Int. *683–684*, 145–161. https://doi.org/10.1016/j.quaint.2023.06.012.
41. Fernández-Palacios, E., Herrera-Herrera, A.V., Gilson, S.-P., Égüez, N., Jambrina-Enríquez, M., Santana, J., and Mallol, C. (2024). Distinguishing between sheep and goat in archaeological fumiers through faecal lipid biomarkers: The case of Belmaco Cave (Canary Islands, Spain). Quatern. Int. *683–684*, 135–144. https://doi.org/10.1016/j.quaint.2023.08.012.
42. Gea, J., Sampedro, M.C., Vallejo, A., Polo-Díaz, A., Goicolea, M.A., Fernández-Eraso, J., and Barrio, R.J. (2017). Characterization of ancient lipids in prehistoric organic residues: Chemical evidence of livestock-pens in rock-shelters since early neolithic to bronze age. J. Sep. Sci. *40*, 4549–4562. https://doi.org/10.1002/jssc.201700692.

43. Vallejo, A., Forgia, V., Vergès, J.M., Gorostizu-Orkaiztegi, A., Alday-Izaguirre, A., Elejaga-Jimeno, A., Sampedro, M.C., Sánchez-Ortega, A., and Barrio, R.J. (2023). Identification of animal species housed and herding practices in ancient sediments from the Vallone Inferno rock-shelter (Scillato, Sicily, Italy) using faecal biomarkers, hormones, and their metabolites. Quatern. Int. *683-684*, 123–134. https://doi.org/10.1016/j.quaint.2023.08.003.

44. Vallejo, A., Gea, J., Gorostizu-Orkaiztegi, A., Vergès, J.M., Martín, P., Sampedro, M.C., Sánchez-Ortega, A., Goicolea, M.A., and Barrio, R.J. (2022). Hormones and bile acids as biomarkers for the characterization of animal management in prehistoric sheepfold caves: El Mirador case (Sierra de Atapuerca, Burgos, Spain). J. Archaeol. Sci. *138*, 105547. https://doi.org/10.1016/j.jas.2022.105547.

45. Vallejo, A., Gea, J., Massó, L., Navarro, B., Gorostizu-Orkaiztegi, A., Vergès, J.M., Sánchez-Ortega, A., Sampedro, M.C., Ribechini, E., and Barrio, R.J. (2022). Lipid Biomarkers as a Tool for the Identification of Herder Activities in El Mirador Cave. In Prehistoric Herders and Farmers: A Transdisciplinary Overview to the Archeological Record from El Mirador Cave, E. Allué, P. Martín, and J.M. Vergès, eds. (Springer), pp. 251–270. https://doi.org/10.1007/978-3-031-12278-1_13.

46. Harrault, L., Milek, K., Jardé, E., Jeanneau, L., Derrien, M., and Anderson, D.G. (2019). Faecal biomarkers can distinguish specific mammalian species in modern and past environments. PLoS One *14*, e0211119. https://doi.org/10.1371/journal.pone.0211119.

47. Prost, K., Birk, J.J., Lehndorff, E., Gerlach, R., and Amelung, W. (2017). Steroid Biomarkers Revisited - Improved Source Identification of Faecal Remains in Archaeological Soil Material. PLoS One *12*, e0164882. https://doi.org/10.1371/journal.pone.0164882.

48. Zocatelli, R., Lavrieux, M., Guillemot, T., Chassiot, L., Le Milbeau, C., and Jacob, J. (2017). Fecal biomarker imprints as indicators of past human land uses: Source distinction and preservation potential in archaeological and natural archives. J. Archaeol. Sci. *81*, 79–89. https://doi.org/10.1016/j.jas.2017.03.010.

49. Bergadà, M.M., Peña, J.L., Serrat, D., Poch, R.M., and Fullola, J.M. (2005). Prospecció geoarqueològica del curs mitjà del Segre (Artesa de Segre, Foradada, Cubells, Alòs de Balaguer, La Noguera) (Tribuna d'Arqueologia 2001-2002), pp. 7–26.

50. Sánchez de la Torre, M., González Olivares, C.B., Gratuze, B., Le Bourdonnec, F.-X., and Mangado, X. (2022). Geochemical Study of Chert Artefacts from Xicotó Rockshelter (NE Iberia) Archaeological Site. New Data on Neolithic and Mesolithic Human Occupations. Nat. Sci. Arch. *13*, 99–115.

51. Bronk Ramsey, C. (2021). OxCal v. 4.4 (software). https://c14.arch.ox.ac.uk/oxcal.html.

52. Reimer, P.J., Austin, W.E.N., Bard, E., Bayliss, A., Blackwell, P.G., Bronk Ramsey, C., Butzin, M., Cheng, H., Edwards, R.L., Friedrich, M., et al. (2020). The IntCal20 northern hemisphere radiocarbon age calibration curve (0–55 cal k BP). Radiocarbon *62*, 725–757. https://doi.org/10.1017/RDC.2020.41.

53. Mentzer, S.M. (2014). Microarchaeological Approaches to the Identification and Interpretation of Combustion Features in Prehistoric Archaeological Sites. J. Archaeol. Method Th. *21*, 616–668. https://doi.org/10.1007/s10816-012-9163-2.

54. Villagran, X., Huisman, D., Mentzer, S., Miller, C., and Jans, M. (2017). Bone and other skeletal tissues. In Archaeological Soil and Sediment Micromorphology, C. Nicosia and G. Stoops, eds. (Wiley), pp. 9–38. https://doi.org/10.1002/9781118941065.ch1.

55. Mangado Llach, X., and Sánchez de la Torre, M. (2014). Memòria de les campanyes 2014 i 2015 a l'Abric del Xicotó (Alòs de Balaguer, La Noguera, Lleida). Memòries d'Intervenció Arqueològica de la Generalitat de Catalunya. http://hdl.handle.net/10687/439060.

56. Mangado Llach, X., and Sánchez de la Torre, M. (2016). Memòria de la campanya 2016 a l'Abric del Xicotó. Memòries d'Intervenció Arqueològica de la Generalitat de Catalunya. http://hdl.handle.net/10687/439062.

57. Stoops, G. (2021). Guidelines for Analysis and Description of Soil and Regolith Thin Sections, Second ed. (Wiley). https://doi.org/10.2136/guidelinesforanalysis2.

58. Canti, M.G., and Nicosia, C. (2018). Formation, morphology and interpretation of darkened faecal spherulites. J. Archaeol. Sci. *89*, 32–45. https://doi.org/10.1016/j.jas.2017.11.004.

59. Bliedtner, M., Schäfer, I.K., Zech, R., and von Suchodoletz, H. (2018). Leaf wax n-alkanes in modern plants and topsoils from eastern Georgia (Caucasus) – implications for reconstructing regional paleovegetation. Biogeosciences *15*, 3927–3936. https://doi.org/10.5194/bg-15-3927-2018.

60. Bush, R.T., and McInerney, F.A. (2013). Leaf wax n-alkane distributions in and across modern plants: Implications for paleoecology and chemotaxonomy. Geochim. Cosmochim. Acta *117*, 161–179. https://doi.org/10.1016/j.gca.2013.04.016.

61. Wiesenberg, G.L.B., Schwarzbauer, J., Schmidt, M.W.I., and Schwark, L. (2004). Source and turnover of organic matter in agricultural soils derived from n-alkane/n-carboxylic acid compositions and C-isotope signatures. Org. Geochem. *35*, 1371–1393. https://doi.org/10.1016/j.orggeochem.2004.03.009.

62. Jambrina-Enríquez, M., Mallol, C., Tostevin, G., Monnier, G., Pajović, G., Borovinić, N., and Baković, M. (2022). Hydroclimate reconstruction through MIS 3 in the Middle Paleolithic site of Crvena Stijena (Montenegro) based on hydrogen-isotopic composition of sedimentary n-alkanes. Quaternary Sci. Rev. *295*, 107771. https://doi.org/10.1016/j.quascirev.2022.107771.

63. Zech, M., Buggle, B., Leiber, K., Markovic, S., Glaser, B., Hambach, U., Huwe, B., Stevens, T., Sumegi, P., Wiesenberg, G., and Zoller, L. (2009). Reconstructing Quaternary vegetation history in the Carpathian Basin, SE Europe, using n-alkane biomarkers as molecular fossils: problems and possible solutions, potential and limitations. Eiszeit. Gegenwart. Quaternary Science Journal *85*, 150–157.

64. Schatz, A.K., Zech, M., Buggle, B., Gulyás, S., Hambach, U., Marković, S.B., Sümegi, P., and Scholten, T. (2011). The Quaternary loess record of Tokaj, Hungary – reconstructing palaeoenvironment, vegetation and climate using stable C and N isotopes and biomarkers. Quat. Int. *240*, 52–61. https://doi.org/10.1016/j.quaint.2010.10.009.

65. Portillo, M., Kadowaki, S., Nishiaki, Y., and Albert, R.M. (2014). Early Neolithic household behavior at Tell Seker al-Aheimar (Upper Khabur, Syria): a comparison to ethnoarchaeological study of phytoliths and dung spherulites. J. Archaeol. Sci. *42*, 107–118. https://doi.org/10.1016/j.jas.2013.10.038.

66. Belarte, M.C., Pastor Quiles, M., Mateu, M., Portillo, M., Saorin, C., Pecci, A., Vila, S., and Gomar, A. (2023). Iron Age combustion structures in the north-eastern Iberian Peninsula: an interdisciplinary experimental study. Archaeol. Anthropol. Sci. *15*, 76. https://doi.org/10.1007/s12520-023-01772-x.

67. Braadbaart, F., Poole, I., Huisman, H.D.J., and van Os, B. (2012). Fuel, Fire and Heat: an experimental approach to highlight the potential of studying ash and char remains from archaeological contexts. J. Archaeol. Sci. *39*, 836–847. https://doi.org/10.1016/j.jas.2011.10.009.

68. Gur-Arieh, S., and Shahack-Gross, R. (2020). Ash and dung calcitic microremains. In Handbook for the analysis of micro-particles in archaeological samples, A.G. Henry, ed. (New York: Springer), pp. 117–147. https://doi.org/10.1007/978-3-030-42622-4_6.

69. Albert, R.M., and Weiner, S. (2001). Study of phytoliths in prehistoric ash layers using a quantitative approach. In Phytoliths: applications in Earth Sciences and human history, J.D. Meunier and F. Colin, eds. (Lisse: Balkema), pp. 251–266.

70. Mas, B., Mangado, X., Sánchez de la Torre, M., Tejero, J.-M., Fullola, J.M., and Allué, E. (2023). Late Paleolithic hunter-gatherers' resilience in the face of the transformation of the vegetation landscape and climate change in the Pre-Pyrenees. Quaternary Sci. Rev. *317*, 108276. https://doi.org/10.1016/j.quascirev.2023.108276.

71. Simoneit, B.R.T., Cox, R.E., Oros, D.R., and Otto, A. (2018). Terpenoid Compositions of Resins from Callitris species (Cupressaceae). Molecules *23*, 3384. https://doi.org/10.3390/molecules23123384.

72. Égüez, N., Mallol, C., and Makarewicz, C.A. (2022). n-Alkanes and their carbon isotopes (δ13C) reveal seasonal foddering and long-term corralling of pastoralist livestock in eastern Mongolia. J. Archaeol. Sci. *147*, 105666. https://doi.org/10.1016/j.jas.2022.105666.

73. Diefendorf, A.F., Mueller, K.E., Wing, S.L., Koch, P.L., and Freeman, K.H. (2010). Global patterns in leaf ^{13}C discrimination and implications for studies of past and future climate. Proc. Natl. Acad. Sci. USA *107*, 5738–5743. https://doi.org/10.1073/pnas.0910513107.

74. Diefendorf, A.F., Sberna, D.T., and Taylor, D.W. (2015). Effect of thermal maturation on plant-derived terpenoids and leaf wax n-alkyl components. Org. Geochem. *89–90*, 61–70.

75. Jambrina-Enríquez, M., Herrera-Herrera, A.V., and Mallol, C. (2018). Wax lipids in fresh and charred anatomical parts of the *Celtis australis* tree: Insights on paleofire interpretation. Org. Geochem. *122*, 147–160. https://doi.org/10.1016/j.orggeochem.2018.05.017.

76. Burguet-Coca, A., Del Valle, H., Expósito, I., Herrejón-Lagunilla, Á., Buitkute, E., Cabanes, D., Cáceres, I., Carrancho, Á., and Villalaín, J.J. (2022). The Fumier Sequences of El Mirador: An Approach to Fire as a Sociocultural Practice and Taphonomic Agent. In Prehistoric Herders and Farmers: A Transdisciplinary Overview to the Archeological Record from El Mirador Cave, E. Allué, P. Martín, and J.M. Vergès, eds. (Springer), pp. 89–110. https://doi.org/10.1007/978-3-031-12278-1_5.

77. Burguet-Coca, A., Polo-Díaz, A., Martínez-Moreno, J., Benito-Calvo, A., Allué, E., Mora, R., and Cabanes, D. (2020). Pen management and livestock activities based on phytoliths, dung spherulites, and minerals from Cova Gran de Santa Linya (Southeastern pre-Pyrenees). Archaeol Anthrop Sci *12*, 148. https://doi.org/10.1007/s12520-020-01101-6.

78. Portillo, M., Dudgeon, K., Allistone, G., Raeuf Aziz, K., and Matthews, W. (2021). The Taphonomy of Plant and Livestock Dung Microfossils: An Ethnoarchaeological and Experimental Approach. Environ. Archaeol. *26*, 439–454. https://doi.org/10.1080/14614103.2020.1800344.

79. Jambrina-Enríquez, M., Herrera-Herrera, A.V., and Mallol, C. (2018). Wax lipids in fresh and charred anatomical parts of the *Celtis australis* tree: Insights on paleofire interpretation. Org. Geochem. *122*, 147–160. https://doi.org/10.1016/j.orggeochem.2018.05.017.

80. Jambrina-Enríquez, M., de Vera, C.R., Davara, J., Herrera-Herrera, A.V., and Mallol, C. (2023). Compound-specific carbon isotope analysis of short-chain fatty acids from Pine tissues: characterizing paleo-fire residues and plant exudates. Archaeol. Anthrop. Sci. *15*, 114. https://doi.org/10.1007/s12520-023-01815-3.

81. Jambrina-Enríquez, M., Herrera-Herrera, A.V., Rodríguez de Vera, C., Leierer, L., Connolly, R., and Mallol, C. (2019). n-Alkyl nitriles and compound-specific carbon isotope analysis of lipid combustion residues from Neanderthal and experimental hearths: Identifying sources of organic compounds and combustion temperatures. Quaternary Sci. Rev. *222*, 105899. https://doi.org/10.1016/j.quascirev.2019.105899.

82. Katz, O., Cabanes, D., Weiner, S., Maeir, A.M., Boaretto, E., and Shahack-Gross, R. (2010). Rapid phytolith extraction for analysis of phytolith concentrations and assemblages during an excavation: an application at Tell es-Safi/Gath, Israel. J. Archaeol. Sci. *37*, 1557–1563. https://doi.org/10.1016/j.jas.2010.01.016.

83. Herrera-Herrera, A.V., and Mallol, C. (2018). Quantification of lipid biomarkers in sedimentary contexts: Comparing different calibration methods. Org. Geochem. *125*, 152–160. https://doi.org/10.1016/j.orggeochem.2018.07.009.

84. Connolly, R., Jambrina-Enríquez, M., Herrera-Herrera, A.V., Vidal-Matutano, P., Fagoaga, A., Marquina-Blasco, R., Marin-Monfort, M.D., Ruiz-Sánchez, F.J., Laplana, C., Bailon, S., et al. (2019). A multiproxy record of palaeoenvironmental conditions at the Middle Palaeolithic site of Abric del Pastor (Eastern Iberia). Quaternary Sci. Rev. *225*, 106023. https://doi.org/10.1016/j.quascirev.2019.106023.

85. Pescini, V., Carbonell, A., Colominas, L., Égüez, N., Mayoral, A., and Palet, J.M. (2024). Neolithic livestock practices in high mountain areas: A multiproxy study of pastoral enclosures of Molleres II (Eastern Pyrenees). Quat. Int. *683–684*, 104–122. https://doi.org/10.1016/j.quaint.2023.04.008.

86. Elhmmali, M.M., Roberts, D.J., and Evershed, R.P. (1997). Bile acids as a new class of sewage pollution indicator. Environ. Sci. Technol. *31*, 3663–3668.

87. Knapp, D.R. (1979). Handbook of Analytical Derivatization Reactions (Wiley).

88. R Core Team (2021). R: A Language and Environment for Statistical Computing (Vienna, Austria: R Foundation for Statistical Computing). https://www.r-project.org/.

89. Zurro, D., García-Granero, J.J., Lancelotti, C., and Madella, M. (2016). Directions in current and future phytolith research. J. Archaeol. Sci. *68*, 112–117. https://doi.org/10.1016/j.jas.2015.11.014.

90. Twiss, P.C., Suess, E., and Smith, R.M. (1969). Morphological classification of grass phytoliths. Soil Sci. Soc. Am. J. *33*, 109–115.

91. Piperno, D.R. (2006). Phytoliths: A Comprehensive Guide for Archaeologists and Paleoecologists (Altamira Press).

92. International Committee for Phytolith Taxonomy ICPT (2019). International Code for Phytolith Nomenclature (ICPN) 2.0. Ann. Bot. *124*, 189–199. https://doi.org/10.1093/aob/mcz064.

93. Miller, J.N., and Miller, J.C. (2000). Statistics and Chemometrics for Analytical Chemistry, 4th Edition (Pearson Education Limited).

STAR★METHODS

KEY RESOURCES TABLE

REAGENT or RESOURCE	SOURCE	IDENTIFIER
Chemicals, peptides, and recombinant proteins		
Dichloromethane Chromasolv® for HPLC grade, purity ≥99.8%	Honeywell	CAS75-09-2
Methanol Chromasolv® for HPLC grade and MeOH, purity ≥99.9%	Honeywell	CAS67-56-1
Hexane Chromasolv® for HPLC grade purity ≥97%	Honeywell	CAS110-54-3
2-Propanol Chromasolv® for HPLC grade, purity ≥99.9%,	Honeywell	CAS: 67-63-0
Diethyl ether for HPLC, purity ≥99%	Acro"s Organics	CAS: 60-29-7
Ethyl Acetate Chromasolv® for HPLC grade, purity ≥97%	Honeywell	
Discovery" DSC-NH2 SPE Bulk Packing	Supelco	Cat#57212-U
Standard mixture C_8-C_{40}, purity ≥90.1%	Sigma-Aldrich	Cat#40147-U
5α-androstane, purity ≥99.9%	Sigma-Aldrich	CAS438-22-2
Dehydroabietic acid, purity >90% LC/MS-ELSD	Sigma-Aldrich	CAS:1740-19-8
N,O-Bis(trimethylsilyl)trifluoroacetamide with trimethylchlorosilane (99%), with 1% Trimethylchlorosidane	Sigma-Aldrich	CAS25561-30-2
Sulfuric acid, purity 95–97%	Honeywell	CAS7664-93-9
Pure quarz sand (50–70 mesh)	Honeywell	CAS14808-60-7
Silica gel (technical grade, pore size 60 Å, 70–230 mesh, 63–200 μm)	Supelco	CAS112-926-00-8
Methyl nonadecanoate (C19:0)	Supelco	CAS1731-94-8
Milli-Q® water	Millipore	CAS7732-18-5
Sodium Polytungstate (SPT)	Sometu Europa	CAS: 12141-67-2
5α-androstan-3β-ol, purity ≥99.9%	Sigma-Aldrich	CAS474-25-9
Hydrochloric acid (≥32%)	SDFCL	CAS: 7647-01-0
Potassium hydroxide, purity ≥85%	Sigma-Aldrich	CAS: 1310-58-3
Acetic acid glacial (100%)	Merck	CAS: 64-19-7
Sodium hydrogen carbonate	Merck	CAS: 144-55-8
Hyocholic acid	Avanti Polar Lipids	CAS: 547-75-1
Cholesterol	Sigma-Aldrich	CAS: 474-25-9
β-Sitosterol	Supelco	CAS: 83-46-5
Coprostanol	Sigma-Aldrich	CAS: 360-68-9
5α-Stigmastanol	Cayman Chemical	CAS: 83-45-4
Cholestanol	Avanti Polar Lipids	CAS: 80-97-7
Hyodeoxycholic acid	Sigma-Aldrich	CAS: 83-49-8
Lithocholic acid	Sigma-Aldrich	CAS: 434-13-9
Ursodeoxycholic acid	Sigma-Aldrich	CAS: 128-13-2
Deoxycholic acid	Sigma-Aldrich	CAS: 83-44-3
Chenodeoxycholic acid	Sigma-Aldrich	CAS: 474-25-9

(*Continued on next page*)

Continued

REAGENT or RESOURCE	SOURCE	IDENTIFIER
Software and algorithms		
MassHunter Workstation	Agilent Technologies	https://www.agilent.com/en/products/software-informatics/masshunter-suite/masshunter-quantitative-analysis
NIST Mass Spectra Database v.14	National Institute of Standards and Technology (NIST)	https://chemdata.nist.gov/
IsoDat 3.0 software	Thermo Scientific	https://www.thermofisher.com/es/es/home/technical-resources/software-downloads.html
R software	The R Foundation	https://www.r-project.org/
R code	Zenodo	https://doi.org/10.5281/zenodo.15756264
GitHub repository	GitHub	https://github.com/Neguez/2025-Xicoto.git
Excel 2019	Microsoft	https://www.microsoft.com/es-es/microsoft-365/previous-versions/microsoft-office-2019
Other		
Furnace TR240	Nabertherm GmbH	https://nabertherm.com/en/products/labor/ovens-and-forced-convection/ovens-electrically-heated CAT#
Ultrasonic bath USC 600th	VWR International	Cat#142-0090
Centrifuge Mega Star 1.6	VWT International	Cat#521-26-59
Nitrogen evaporator (RapidVap® Vertex Evaporator)	Labconco	Cat#7320037
pHmeter Sension+ PH3	Hach	Cat#LPV2021T.98.002
Vortex Genie 2	Scientific Industries	Cat#SI-0256
Nitrogen evaporator (24 positions N-EVAP)	Organomation Associates Inc.	Cat#11250
Nikon Eclipse E200 polarizing microscope	Nikon Instruments Inc.	https://www.microscope.healthcare.nikon.com/products/upright-microscopes/eclipse-e200
Olympus BX53 polarizing microscope	Olympus IMS	https://www.olympus-ims.com/en/microscope/bx53m/
Agilent 7890B GC	Agilent Technologies	https://www.agilent.com/en/product/gas-chromatography/gc-systems/7890b-gc-system
Agilent 5977A MSD	Agilent Technologies	https://www.agilent.com/en/promotions/gc-gcms-resolve
Agilent HP-5ms capillary column: length: 30 m, ID: 250 mm, 0.25 mm film thickness	Agilent Technologies	Cat#19091S-433UI
Thermo Scientific Isotope Ratio Mass Spectrometer Delta V Advantage	Thermo Scientific	https://www.thermofisher.com/es/es/home/industrial/mass-spectrometry/isotope-ratio-mass-spectrometry-irms/gas-isotope-ratio-mass-spectrometry-irms.html
GC Trace1310	Thermo Scientific	Cat#PGA000010011
Conflo IV	Thermo Scientific	Cat#IQLAAEGAATFAETMAXB
GC Isolink II	Thermo Scientific	Cat#IQLAAEGAATFAETMATA
Portable pH meter Elite PCTS	Thermo Scientific	ELITEPCTS

EXPERIMENTAL MODEL AND SUBJECT DETAILS

This study does not use experimental models.

METHOD DETAILS

Soil micromorphological analysis

The micromorphological sample was processed by the Thin Section Service (Faculty of Earth Sciences, University of Barcelona; see the web page at https://www.ub.edu/portal/web/ciencies-terra/lamina-prima) into two thin sections (EC3-1 and EC3-2), which were analyzed in plane-polarized light (PPL), cross-polarized light (XPL), and blue light (BL) using petrographic microscopes (Nikon E600-POL, Nikon AZ100, Leica DM2700P). Descriptions followed standard guidelines proposed by Stoops.[57]

Analysis of calcitic and siliceous microremains: Fecal spherulites, ash pseudomorphs and phytoliths

For the extraction and quantification of fecal spherulites and ash pseudomorphs, we followed Gur-Arieh et al.[36] Around 50 mg of bulk sediment were passed through a 150 μm sieve, and placed into a 2 mL Eppendorf tube. 500 μL of 2.4 g/mL Sodium Polytungstate (SPT) were then added. Tubes were then vortexed (3 s) and sonicated for 10 min. After shortly applying vortex again, 50 μL of solution was immediately placed onto a microscope slide and covered with coverslip (24 × 24 mm).

As for the extraction of phytoliths, 50–60 mg of sediment were burned at 500°C for 4 h due to the high amount of organic material. Then we followed Katz et al.[82] rapid extraction. The remaining sediment was weighed and processed using 50 μL of 6N HCl to remove carbonates. Once the reaction with HCl stopped, 450 μL of sodium polytungstate solution (SPT, 2.4 g/mL) was added, vortexed, and sonicated for 10 min. Samples were then centrifuged for 5 min at 6000 rpm, and the supernatant was transferred to a new Eppendorf tube. 50 μL of supernatant were mounted on slides and covered with 24 × 24 mm cover slips.

Biomarker analysis

The biomarker analysis targeted *n*-alkanes and steroids. 10 g of each sample were oven-dried for 48 h at 60°C and homogenized. Extraction protocol followed Herrera-Herrera and Mallol[83] and Connolly et al.[84] for *n*-alkanes (5 g); and Pescini et al.[85] and Fernández-Palacios et al.[41] for sterols, stanols, and bile acids (5 g).

n-Alkanes were extracted in 40 mL of dichloromethane/methanol (DCM:MeOH 9:1 v/v) through three sonication (30 min), centrifugation (10 min at 4700 rpm), and filtration (glass wool) cycles to obtain the total lipid extract (TLE). After evaporation, the TLE was subsequently reconstituted with DCM, and *n*-alkanes were eluted with hexane ($^3/_8$ dead volume (DV)) using silica gel columns (1 g silica 70–230 mesh and 0.1 g sand 50–70 mesh).

Steroids were extracted with 40 mL of dichloromethane:methanol (DCM:MeOH 2:1 v/v) and we followed the same protocol as described above to obtain the TLE. Samples were then saponified following Elhmmali et al.[86] with some modifications. We added 5 mL of potassium hydroxide solution (5M) in MeOH 90% v/v to the sample TLE for alkalization and hyocholic acid (3 μL) as an internal standard. Samples were then heated at 100°C for 60 min. 22 mL of distilled Milli-Q water were then added and samples were acidified using a hydrochloric solution (6 M) to obtain a pH value of 3–4. Steroids were then extracted in three cycles by adding 10 mL DCM (total of 30 mL DCM) and mixing with vortex (1 min). Following this, polymerically bonded aminopropyl phase columns (500 mg sorbent), previously activated with 6 mL *n*-hexane, were used for solid phase extraction. Evaporated samples were transferred into the columns by reconstitution with 1 mL *n*-hexane. For the elution of sterols/stanols we used 6 mL of DCM/2-propanol (2:1 v/v), while the elution of carboxylic acids was achieved using 12 mL of 3% v/v acetic acid in diethyl ether. Carboxylic acids were derivatized by methylation, for which 5 mL MeOH and 400 μL H_2SO_4 were added and samples were heated at 70°C for 240 min to obtain methyl esters. Following this, samples were neutralized with 10 mL of a saturated bicarbonate solution. The extraction of methyl esters was carried out by adding 3 mL *n*-hexane and using vortex (1 min). This was repeated three times (total of 9 mL), and then samples were dried using nitrogen. Methylated carboxylic acids were then fractionated, this time through silica gel columns (600 mg sorbent). Sample introduction into the columns took place after reconstitution using 1 mL 2:1 v/v DCM/hexane. Through elution with 5 mL 2:1 v/v DCM/hexane we obtained monocarboxylic fatty acids methyl esters, while hydroxycarboxylic acid methyl esters (encompassing bile acids) were eluted with 5 mL 2:1 v/v DCM/MeOH. Finally, eluted fractions were again evaporated under a gentle nitrogen flow.

n-Alkanes were directly injected after the addition of the internal standard (IS): 1 μL of 5α-androstane 400 mg/L was added in the reconstituted sample with 50 μL DCM. Steroid fractions (sterols/stanols and hydroxycarboxylic acids) were silylated and injected in less than 24 h.[87] The latter were dissolved with DCM, mixed with 100 μL of N,O-Bis(tri-methylsilyl)trifluoroacetamide (BSTFA) + trimethylchlorosilane (TCMS) 99:1 v/v, and 1 μL of 5α-androstan-3-ol (400 mg/L) as IS was also added. Derivatization involved 60 min of heating (80°C) to obtain trimethylsilyl (TMS) ethers. Samples were dried and redissolved with 50 μL DCM prior to injection. Two replicates from each fraction (*n*-alkanes, sterols/stanols and hydroxycarboxylic acids) were injected.

Instrumental analysis

Compounds were determined by Gas Chromatography-Mass Spectrometry (GC-Agilent 7890B, MSD Agilent 5977A). The chromatograph is equipped with a bonded fused silica HP-5ms capillary column ((5%phenyl)-methylpolysiloxane, 30 m, ID: 250 μm, film thickness 0.25 μm), an electron impact interface (equipped with multimode injector (MMI)), and an automatic autosampler. The GC oven temperature is initiated at 70°C (for 2 min) with a heating rate of 12 °C/min until reaching 140°C, and to a final temperature of 320°C at a rate of 6°C/min (for 16 min), using Helium as carrier gas (1 mL/min). The MMI was held at a split ratio of 5:1 with an initial temperature of 70°C for 51 s, then heated to 300°C at a rate of 720 °C/min. As for the MS conditions, the Q operated

in a full-scan mode with m/z ranging from 40 to 580. Electron ionization energy was set at −70 eV. The temperature for the ion source was set at 230°C. Q temperature at 150°C. To avoid damage to the mass source filament solvent delay was programmed to 7 min. MassHunter Workstation software (Agilent Technologies) was used for equipment control and for data acquisition and processing.

Compound-specific stable carbon isotopes

Carbon isotope analysis by GC-IRMS was performed using a Thermo Scientific Isotope Ratio Mass Spectrometer Delta V Advantaged coupled to a GC Trace1310 through a Conflo IV interfaced with a temperature converter GC Isolink II. Samples were injected (1 μL) by means of a Programmable Temperature Vaporizer (PTV) injector in splitless mode, with the temperature increasing from 79°C (held 0.5 min) to 325°C (held 3 min) at a rate of 10°C·s^{-1} and finally to 350°C (held 3 min) at 14°C·s^{-1}. The GC was fitted with a Trace Gold 5-MS (Thermo Scientific) fused silica capillary column (30 m length x 0.25 mm i.d., 0.25 μm film thickness). Helium was the carrier gas at a flow rate set at 1.5 mL min^{-1}. The combustion reactor temperature was maintained at 1000°C. The GC oven temperature program comprised a 2 min isothermal period at 70°C increasing to 140°C (held 2 min) at a rate of 12°C·min^{-1}, followed by an increase period to 320°C (held 15 min) at 3°C·min^{-1}. Data acquisition and processing were carried out using the Isodat 3.0 software (Thermo Scientific). δ^{13}C values were standardized to VPDB (Vienna Pee Dee Belemnite) scale using an *n*-alkane Schimmelmann type A6 mixture (nC_{16} to nC_{30}). Certificate of analysis indicates that data for *n*-alkane Schimmelmann type A6 mixture have a precision of ±0.05‰ for δ^{13}C. Reproducibility was better than ±0.5‰ for carbon isotope measurements.

Data visualization

Data visualization was performed with Microsoft Excel and R software.[88]

QUANTIFICATION AND STATISTICAL ANALYSIS

Microremains

Counting of fecal spherulites, ash pseudomorphs, and phytoliths was carried out at 400× magnifications in 30 random fields of view. Phytolith morphological analysis was performed by identifying a minimum of 250 morphotypes per sample.[89] For phytolith identification, we used standard literature,[90,91] and we followed the International Code of Phytolith Nomenclature 2.0.[92] A Zeiss Axiolab 5 microscope was used for phytolith, fecal spherulite, and ash pseudomorph analyses.

Biomarkers

Compounds were identified by comparison of their retention times and mass spectra with those of reference compounds, by comparison with the NIST mass spectra library, and peak signals of specific ion fragments. *n*-Alkanes and steroids were quantified, expressed as microgram per gram of dry sample (μg/gds), using calibration curves (see key resources table for used standards), obtained from the relation of area/arealS against the concentration of target compounds dissolved in the solvent.

The uncertainties associated with the concentrations presented in Table 6 were calculated based on the error using confidence intervals expressed as $x_0 \pm t(n-2,\alpha)\, S_{x_0}$ for a 95% confidence level. The following equation was used[93]:

$$S_{x_0} = \frac{S_{y/x}}{b}\sqrt{1+\frac{1}{n}+\frac{(y_0-\bar{y})^2}{b^2\sum_i (x_i-\bar{x})^2}}$$

S_{x_0} is the standard deviation of the concentration; $S_{y/x}$ the error of the estimate; b the slope of the calibration curve; n the number of concentration levels used to construct the calibration curve; y_0 the signal value for the sample of interest; $\bar{y}$ the mean signal value of the calibration curve; x_i the individual concentration values of the curve; and $\bar{x}$ the mean concentration value.

Statistical analysis

A Shapiro-Wilk test was performed without considering the control sample to check the assumption of normality for our isotopic dataset (see *Results* section), with data showing a p-value >0.05. An ANOVA analysis was used to compare the means of our groups of samples, with no significant differences observed between them (p-value = 0.8465). A post hoc Tukey test for group-pairing analysis also did not show any significant results (MR-MB p-value = 0.9216992, MW-MB p-value = 0.8568542, MW-MR p-value = 0.9880570).